Journal of Magnetism and Magnetic Materials 627 (2025) 173132

Contents lists available at ScienceDirect

Journal of Magnetism and Magnetic Materials

journal homepage: www.elsevier.com/locate/jmmm

Review Article

M-type hexaferrites: A review of the impact of rare earth substitution on magnetic properties

A. Lobo-Guerrero [a,*], V.E. Salazar-Muñoz [b], R.H. Aguilera Del Toro [c], E.E. Hernández-Vázquez [d]

[a] Área Académica de Ciencias de la Tierra y Materiales, Universidad Autónoma del Estado de Hidalgo, Carr. Pachuca-Tulancingo km. 4.5, 42184, Mineral de la Reforma, Hidalgo, Mexico
[b] Facultad de Ingeniería, Universidad Autónoma de San Luis Potosí, Av. Manuel Nava 8, 78290 San Luis Potosí, S.L.P., Mexico
[c] Departamento de Física Teórica, Atómica y Óptica, Universidad de Valladolid ES-47011 Valladolid, Spain
[d] Facultad de Ciencias Químicas, Universidad Autónoma de Chihuahua, Circuito Universitario s/n, Campus Chihuahua II, 31125 Chihuahua, Mexico

ARTICLE INFO

Keywords:
Rare earth
M-type hexaferrite
Rare earth substitution
Hard magnetic properties
Synthesis methods

ABSTRACT

The substitution of rare earths in M-type hexaferrites has attracted attention in the past decade due to their ability to modify the crystal structure and magnetic properties. However, achieving rare earth incorporation in the M-type structure is extremely challenging because they often create secondary phases during the sintering process. This study analyzes the effect of rare earth substitution on the magnetic properties of M-type hexaferrites, examining 312 samples reported in the last decade. We focus on the effects of rare earth substitution on the magnetic properties, including magnetization to saturation, remanence magnetization, coercive field, remanence squareness ratio and maximum energy product. Moreover, different fabrication routes and sintering parameters such as heating time and temperature were considered in the analysis. The results are presented in a comprehensive table showcasing the progress that rare earth-substituted hexaferrites have made in the last decade. This review provides insights into the correlations between experimental factors and synthesis parameters with purity, structural variations and the magnetic properties resulted from the rare-earths substitution. This review aims to elucidate the connections between synthesis parameters and experimental factors, with the resulting purity, structural variations, and magnetic properties of M-type hexaferrites substituted using rare-earths. In addition, a critical perspective is presented about the challenges and potential of substituted hexaferrites in the next-generation of magnetic ceramics.

1. Introduction

M-type hexaferrites belong to the family of ferrimagnetic oxides with the same crystalline structure as the Magnetoplumbite mineral ($PbFe_{7.5}Mn_{3.5}A_{0.5}O_{19}$) [1]. The M-type hexaferrites were first synthesized in 1951 by the Philips company which developed a ceramic compound named ferroxdure ($BaFe_{12}O_{19}$) [2,3]. Since its discovery, these hexaferrites have been the subject of increasing research interest in magnetic materials area [4]. These magnetic oxides showed a ferrimagnetic arrangement with a large saturation magnetization, magnetic anisotropy, as well as coercive field, making them ideal materials for a wide range of applications [5,6].

M-type hexaferrites are inorganic compounds consisting of a hexagonal close packing (HCP) of oxygen anions, where one oxygen is replaced by a divalent cation (Me), usually Me = Sr^{2+}, Ba^{2+} or Pb^{2+}. This HCP structure enables five non-equivalent interstitial sites: 2a, $4f_2$ and 12 k octahedrally coordinated, $4f_1$ tetrahedrally coordinated; and 2b penta-coordinated to form a bipyramidal site [7]. The M-type arrangement allows for substituting the divalent cation by other divalent or trivalent cation to form a solid solution limited by chemical and physical factors. Therefore, the substitution occurs if Goldschmidt's rules are satisfied [8]. Over the years many substitutional hexaferrites have been developed for both the divalent cation and the interstitial iron cations [9]. However, substituting cations of the hexaferrite structure can result in significant changes in the magneto-structural anisotropy [10].

The substitution of rare earth cations in the M-type structure was first conceived in the middle 50′s. Summergrad and Banks attempted to

* Corresponding author.
E-mail addresses: azdrubal_guerrero@uaeh.edu.mx (A. Lobo-Guerrero), veronica.salazar@uaslp.mx (V.E. Salazar-Muñoz), rodrigohumberto.aguilera@uva.es (R.H.A. Del Toro), esther.hernandez@ipicyt.edu.mx (E.E. Hernández-Vázquez).

https://doi.org/10.1016/j.jmmm.2025.173132
Received 13 January 2025; Received in revised form 14 April 2025; Accepted 29 April 2025
Available online 3 May 2025

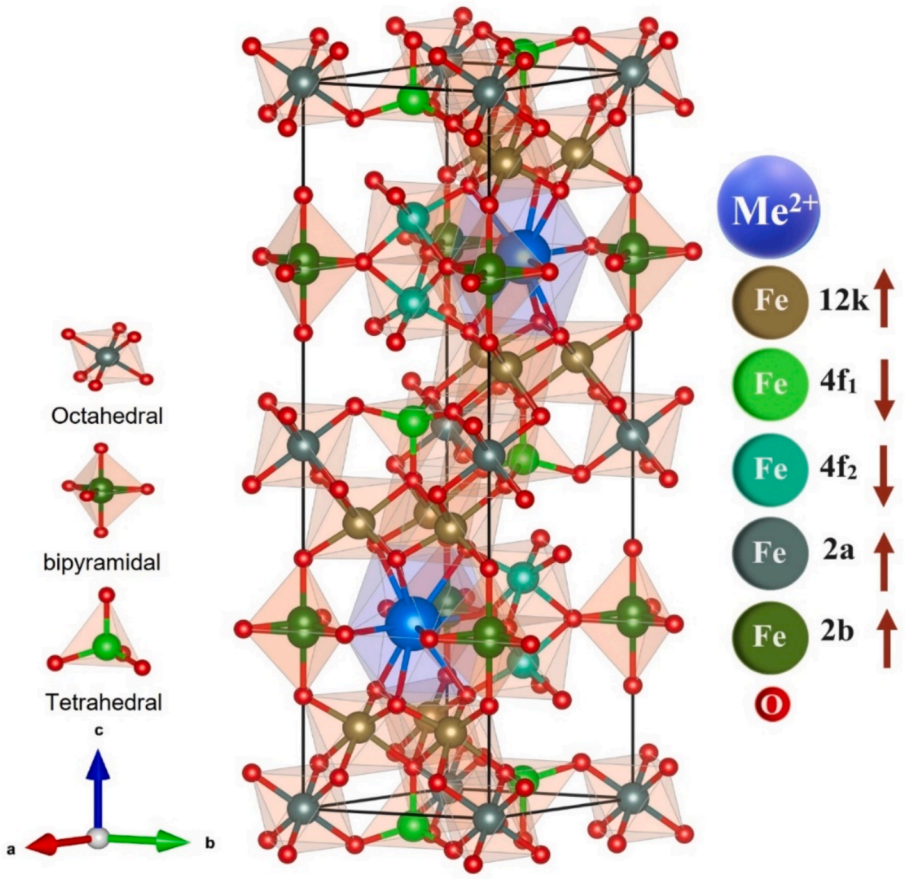

Fig. 1. Crystalline structure of the M-type hexaferrite.
Source: Elaborated by authors using VESTA

develop a lanthanum-based M-type hexaferrite [11]. Then, Deschamp and Bertaut worked on the substitution of rare earths for barium in hexagonal ferrites [12]. In the early 50′s, Moruzzi and Shafer managed to manufacture lanthanum hexaferrite and study the phase stability [13]. In 60′s Aharoni and Schieber determined the magnetic moment of lanthanum hexaferrite. They concluded that a divalent iron close to lanthanum site should reduce the magnetic moment by one Bohr magneton as compared to a trivalent iron ion which explained a drop observed on the magnetization saturation of the lanthanum hexaferrite regarding the barium one [14]. After in the early 1970s, Frantsevich and Tul'chinskii investigated the impact of small amounts of lanthanum on electrical and magnetic properties of M-type hexaferrite [15]. Lotgering and Van Diepen revealed the effects of lanthanum on the structure and demonstrated the occurrence of superexchange interactions between Fe^{3+} and Fe^{2+} [16,18,17]. From that point, the substitution of various other rare earth elements was investigated. For example, in the 80′s Kirichok et al. observed variations in the maximum energy product $(BH)_{max}$ when praseodymium (Pr) was substituted in the hexaferrite. This effect was attributed to alterations in the hexaferrite's electronic structure which also affect its anisotropy field [19]. They also studied the hexaferrites' substitution with various rare earths to assess the effects on their magnetic properties [20]. These early studies laid the groundwork for the exploration of rare earth impact on the magnetic properties of M-type hexaferrites [21].

This critical review analyzes the impact of rare earth substitutions on the magnetic properties of M-type hexaferrites. Based on studies conducted over the past decade by various research groups, data from 312 samples have been collected. A comprehensive data analysis enabled the identification of the influence of rare earth substitution and synthesis process on the magnetic properties crystalline structure, microstructural changes, and phase composition of the substituted hexaferrites. Additionally, this review assesses the challenges and novel opportunities of the rare earth substitution in the improvement of the magnetic yield of the M-type hexaferrites.

2. Magnetic and crystalline structure

To understand the magnetic properties of the hexaferrite family compounds, it is necessary to investigate their structural aspects. M-type hexaferrites are a specific type of iron-based compound that have a hexagonal crystal structure. The name is given because of the hexagonal arrangement and the stacking of various magnetic substructures along the c-axis. The M-type hexaferrite is formed by a stacking sequence described in terms of two structural blocks: the spinel "S" block $(Fe^{3+}{}_2Fe^{3+}{}_4O^8)^{2+}$ and the "R" block $(MeFe_6O_{11})^{2-}$ [1,6]. In particular, the stacking sequence of the M-type hexaferrite is SRS*R*, where * denotes a rotation of 180° about the c-axis. M-type hexaferrites crystallize with hexagonal symmetry and $P6_3/mmc$ space group, consisting of two units of the formula $MeFe_{12}O_{19}$ (Me = Ba, Sr, Pb, Ca) with 24 iron atoms (Fe^{3+}) located at five interstitial sites: three octahedral (12 k, 2a, and $4f_{II}$), one tetrahedral ($4f_I$), and one bipyramidal (2b). The divalent metal ion (Me^{2+}) is located in the octahedral sites of the open tetrahedral layers.

Fig. 1 shows the hexagonal unit cell of the M-type hexaferrite, consisting of lattice parameters a = b, and c being significantly larger than a. The larger Me^{2+} and O^{2-} ions are in a close-packed structure, while the smaller Fe^{3+} ions occupy the interstitial sites. The structural configuration of the iron cations in the structure of M-type ferrites results in a

specific arrangement of magnetic moments. The magnetic moments of the iron cations are aligned parallel or antiparallel to the crystallographic c axes, resulting in a ferrimagnetic structure [1–4]. This magnetic compound shows high magnetocrystalline anisotropy. The magnetocrystalline anisotropy is an intrinsic property of a magnetic material that causes its magnetization to align itself along a preferred crystallographic direction. The magnetocrystalline anisotropy arises from the interaction of the spin magnetic moment with the crystal lattice (spin–orbit coupling), which gives rise to easy and hard magnetization directions [22,23]. The application of an external magnetic field causes a preferential orientation of electron spins along the field direction. Consequently, the orbit of the electron tries to follow this reorientation. However, the strong spin–orbit coupling to the crystal lattice hinders the rotation of the spin axis [22]. The spin–orbit coupling is particularly strong in M-type hexaferrites and substitutions could activate different single-ion or collective contributions in the crystalline lattice. Most type of substitutions cause a drastic reduction of the magnetocrystalline anisotropy, and consequently a reduction of the energy product [24]. However, some rare earth substitutions can increase the magnetocrystalline anisotropy with decreasing temperature, probably due to formation of Fe^{2+} in octahedral sites [23,24].

The ferrimagnetic nature of the M-type hexaferrite arises due to the parallel and antiparallel alignment of the spin orientation of Fe3+ ions. Each one of the iron cations Fe^{3+} show a net magnetic moment of 5 μ_B distributed five distinct iron sublattices: three parallel to the crystallographic c-axes: 12 k (↑), 2a (↑), and 2b (↑), and two antiparallel: $4f_1$ (↓) and $4f_2$ (↓), see Fig. 1. This magnetic arrangement results in the annulment of parallel and antiparallel magnetic moments. However, the number of parallel magnetic moments is larger than the antiparallel ones by eight, resulting in a net magnetic moment of 40 μ_B per unit cell.

In the hexaferrites, the magnetic moment of two iron cations is coupled through an oxygen anion, in a mechanism established as superexchange interactions and strongly controlled by magnetocrystalline anisotropy. The superexchange interactions are represented as Fe^{3+}–O^{2-}–Fe^{3+} and play a crucial role in the magnetic properties of hexaferrite [25]. Besides, the substitutional elements can affect the structure of the hexaferrite, which instead affect the magnetocrystalline anisotropy and the superexchange lengths Fe^{3+}–O^{2-}–Fe^{3+}, promoting a canting rotation of the magnetic moment and a reduction of the net magnetization properties of the hexaferrite.

The magnetic properties of M-type hexaferrites are susceptible to change when a cation within its structure is replaced by a foreign divalent or trivalent cation. Specifically, substitution with rare earth atoms can affect superexchange interactions and magnetocrystalline anisotropy, modify the electronic structure and structural properties, resulting in a change of the magnetic properties [26]. Additionally, rare earth atoms may possess different magnetic moments that must be considered. It is important to note that the effects of rare earth substitution in the magnetic properties of the M-type hexaferrites vary depending on the specific element, substitutional procedure employed and other factors such as synthesis method, crystallinity, particle size, and homogeneity.

3. Synthesis of the rare earth substituted hexaferrites

Hexagonal ferrites can be obtained from a variety of chemical and physical fabrication methods. These methods usually involve a (or close to) stoichiometric mix of chemicals, for example oxides, carbonates or hydroxides among other compounds, followed by a heat treatment required to crystallize the M-type structure. Chemical methods allow the synthesis of hexaferrite nanoparticles at very low temperatures whereas by physical methods usually higher sintering temperatures are required affecting on the particle's growth. The fabrication method has an enormous impact on the structural and magnetic properties of the hexaferrite compounds. For example, low sintering temperatures used by the chemical methods allow to obtain low particle size with a very homogeneous distribution, from which it is expected high coercive fields but probably low magnetizations resulting from a poor crystallization. On the other hand, increasing the sintering temperature results in a fall of the coercive field due to the growth of particle size usually accompanied by a broad particle size distribution. However, crystallinity of M-type compound becomes higher, and the magnetizations usually increase.

The sintering temperature is an important factor for the complete reaction of the chemical precursors, if low sintering temperature is employed, it could be remained hematite (Fe_2O_3) as the second minor phase. However, at higher temperatures, the crystallization of hexagonal ferrites type X can be reached. The substitution of rare earths in the structure of the M-type hexaferrite usually requires higher sintering temperatures than the ones necessary for obtaining the hexaferrites without substituents. This condition is necessary due to the rare earths tending to form orthoferrite phases at sintering temperatures very close to the ones required for sintering the M-type hexaferrite. In many cases, the presence of magnetic rare earth orthoferrite phase is not clearly recognizable because the small amount of rare earth used as substituent and because the main peaks of rare earth orthoferrites overlap with the main peaks of the M-type hexaferrite. Besides, the presence of magnetic rare earth orthoferrites with the M-type hexaferrites could improve the magnetic properties by synergic combination between both phases.

Other key point related to rare earth involves the site substitution of the rare-earth elements within the hexagonal $P6_3/mmc$ crystalline structure. According to the literature, rare earth elements (Re^{3+}) can partially replace the divalent cation (Ba^{2+}, Sr^{2+}, Pb^{2+} or Ca^{2+}) or substitute iron cations (Fe^{3+}) of at least one of the five interstitial sites. The scenario is complex, however, apparently the selected method, the fabrication conditions, stoichiometry as well as the type of rare earth used as substituent element could determine if a rare earth substitutes for the divalent cation or to interstitial iron cations. Obviously, the determining factor is the solubility of the rare earth in the crystalline structure of the M-type hexaferrite.

A summary of each one of the fabrication methods with the most important details recently reported for the synthesis of rare earth substituted hexaferrites is provided in this section. Furthermore, in the supplementary information are presented detailed block diagrams for each one of the fabrication methods.

- **Co-precipitation method (CP)**. In this method, stoichiometric amounts of chloride salts are dissolved in deionized water and stirred to homogenize the solution. 10 M NaOH solution was then slowly added drop wise to the mixture under rigorous stirring. The alkali addition was continued till the pH value of the solution was achieved 12 and was left undisturbed for a few hours for a complete digestion. The precipitates were filtered and washed repeatedly with water and lastly with alcohol. Finally, dried powder is sintered to reach the M-type phase [27,28].
- **Solid-state method (SS).** Stoichiometric amounts of oxides and/or carbonates can be used as raw materials. Then, the powders are wet mixed in alcohol or acetone until homogenized them. A pre-sintering heat treatment can be done to promote primary reactions. Furthermore, a sintering heat treatment between 1250 to 1350 °C is carried out to form the hexaferrite phase [29,30].
- **Citrate precursor-based sol gel process (CT-SG).** High purity nitrate salts are used as chemicals. Citric acid is used as fuel for self-igniting reaction. The stoichiometric ratio of citric acid to metal cations is kept being 1:3. Then, a gel-like substance is obtained after stirring the mixture in deionized water for various hours. Once dried into an oven, the as-obtained ash powder is grinded for its sintering [31,32].
- **Proteic Sol-gel method (P-SG).** Different amounts of nitrate salts are mixed in the stoichiometric ratio and dissolved in filtered coconut water under agitation to achieve a complete homogenization to form the sol. The solution is kept at 100 °C for 24 h for evaporation

and xerogel formation. The xerogel is grounded and calcined at 500 °C to remove all organics residues. Finally, the powder cooled and homogenized, is calcined to crystalize the M-type compound [33,34].

- **Ammonium nitrate melt (ANM).** Appropriate amounts of oxide and/or carbonate powders are mixed and put into melted ammonium nitrate. The solution was stirred in a hot plate until the liquid phase disappeared. Then, isopropyl alcohol is added for a wet grinding stage. Remained organics can be removed calcined between 400–500 °C. Once cooled powder can newly grounded before its thermal treatment for crystallize the M-type hexaferrite phase [35].
- **Sol-gel (SG).** Nitrate salts and citric acid (other acids also can be used with citric acid) are employed as the chemicals, while ammonia (NH_3) solution is employed to adjust the pH. Citric acid is used as a complexing agent to dissolve various compounds in several beakers using deionized water. With the introduction of NH_3 liquid drop by drop, the pH of the solution is maintained at 7. Afterward, the solution is stirred at 100 °C until a wet gel is formed. Then, the dried gel is burned, and the product is grounded and sintered to form hexaferrite nanoparticles [36].
- **Sol-gel auto combustion method (SG-AC).** Nitrate salts and citric acid are mixed in appropriate stoichiometric amounts at 80 °C. The solution was adjusted to pH 8 by adding liquid ammonia and stirred until the combustion started. After the combustion process the powder is grinded and annealed to obtain the M-type hexaferrite compound [37].
- **Oxide One Pot Synthesis (OOPS).** Appropriate nitrate salts are dissolved in the homogeneous solution of ethylene glycol and triethanolamine at 100 °C with stirring. The obtained solution is heated to 120 °C for 2 h, then washed with ethanol and filtered. The remaining sediment is calcined to obtain the hexaferrite compound [38].
- **High-energy milling (HEM).** Chemical precursors are mixed in a stoichiometric ratio in alcoholic media. The wet mix is milled using hard material balls. Several parameters can be optimized in this method, such as the mass ratio of the sample to the balls, rotation speed and time of milling. Once milled, the obtained mud is dried, and the resulting powder is calcined to react the chemicals to form the hexaferrite phase [39].
- **Hydrothermal (HT).** Stoichiometric amounts of nitrates and/or chlorides are mixed in deionized water. 2 M NaOH solution is prepared separately and added drop wise to form the precipitates at pH 14. The mixture is stirred and subsequently sealed in an autoclave maintained at 180 °C for 24 h. Once cooled, the mixture is washed several times with deionized water and ethanol to eliminate impurities. The particles are separated from the solution through centrifugation and further they are dried. Finally, the obtained powder is grinded and annealed to obtain the hexaferrite phase [40].
- **Sol-gel Pechini method (SG-PC).** This method requires the preparation of a polymeric resin from organic acids to obtain a three-dimensional polymeric network. Nitrate salts, citric acid, and ethylene glycol are required for the hexaferrite obtention. The salts are weighted according to hexaferrite stoichiometry and dissolving in deionized water with citric acid in a molar ratio of 5:1. The resultant solution is heated at 70 °C for dehydration and later further heated at 100 °C for polymerization. The resin is heated at 370 °C for 45 min and grounded in an agate mortar and pestle. Finally, the powders are sintered to obtain the hexaferrite phase [41].
- **Tartrate precursor (TP).** Chloride and nitrate salts and tartaric acid are used in the preparation of hexaferrite. Tartaric acid acts as chelating agent and as fuel. The salts are dissolved in deionized water and then the tartaric acid is incorporated and the volume of the mixture adjusted to 500 mL. The solution is stirred at 80 °C to homogenize the components until dried. Then, the gel is heated at 110 to evaporate the remaining water and to produce the gelling mass precursors. These precursors are further heated at high temperature to reach the M-type hexaferrite phase [42].
- **Molten salt via sol–gel (MS-SG).** The hexaferrite were first synthesized using the sol–gel method using citric acid with a molar ratio of 1:1 to the nitrates in aqueous solution, adjusting the pH to 7 using ammonia solution. The mixture is stirred and water slowly evaporated to form a gel. This gel is dried and then self-propagating combusted in air. Afterward, the products are mixed with Na_2SO_4 in a weight ratio of 1:1, this powder is calcined with molten salt assistance in a furnace at a selected temperature to crystallize the hexaferrite phase. Finally, the obtained powders are washed several times with distilled water until the SO_4 is completely removed [43].
- **Spark plasma sintering (SPS).** The hexaferrite compound is prepared by the conventional ceramic method using oxide or carbonate powder at the required stoichiometry. Powders are first pre-heated at 1000 °C and then sintered in a spark plasma sintering apparatus. The pre-sintered powder is placed in a cylindrical graphite die. The die was then placed inside the chamber of the spark plasma sintering apparatus and sintering was formed under vacuum (10–30 Pa). After the spark plasma sintering, the sample is naturally cooled and removed from the die [44].
- **Auto combustion (AC).** Stoichiometric amounts of nitrates, glycine and urea are used for the hexaferrite obtention. A petri dish containing the solution of precursor mixture is heated at 600 °C. The solution begins to boil in the furnace and heat reduction and ignition, followed by a decomposition. When the solution reaches its self-ignition point, it begins to burn, releasing a large amount of heat, burning and forming a fluffy with loose powder. A smoldering combustion occurs with an ignition reaction time between 15 to 18 s, which leads to better homogeneity. The resulting powder is ground, mixed, and calcined to form the hexaferrite phase [45].
- **Sol-gel microwave-assisted synthesis method (MW).** Powder precursors are initially prepared using the traditional sol gel method. Afterward, self-combustion reaction is ignited at 175 °C. The obtained powder contains the hexaferrite precursor is calcined at 800 °C for 80 min in a microwave furnace, using a heating rate of 40 °C/min to obtain the hexaferrite phase [46].
- **Sonochemical method (SCH).** Salt nitrates were used as raw materials. Using a two-step process, ferrite nanoparticles are synthesized by using a combustion process after the sonochemical treatment to produce the nanoparticles. In the first step, 20 g polyethylene glycol-PEG is utilized to dissolve nitrate salts. Then, the solutions are treated using a Hielscher UIP1000 Hdt high-intensity ultrasound homogenizer for 3 min (130 W, 19 kHz), that is equipped with a Bs4d22 ultrasonic block sonotrode (D: 22 mm). During the dispersion process, the mixture darkened and turned to a brownish-red color, indicating the creation of metal hydroxides. During the combustion stage, the colloid systems within the PEG-based structure were subjected to heat in a furnace at 1000 °C under an air atmosphere. This process led to the creation of colloid systems. Following the burning of the PEG and the dehydration of the metal hydroxide nanoparticles, the hexaferrite structures are obtained [47].
- **Polymer precursor method (PPM).** Nanocrystalline hexaferrite powders are prepared using acetate trihydrate ($Me(CH_3COO)_2$ 3H2O) and ferric acetylacetonate ($C_{15}H_{21}FeO_6$) as starting materials. A clear solution is prepared by dissolving 0.5060 g of acetate trihydrate in 15 mL glycerin. The solution is distilled in a rotary evaporator at 120 °C for 1 h to remove the water trapped. The distilled solution is stored in a 50 mL flask, which is moved into a glove box. To prevent the hydrolysis of ferric acetylacetonate, dissolved 4.2381 g of ferric acetylacetonate in a mixture solution of 100 mL anhydrous ethanol and 70 mL acetone in a 250 mL three-neck flask. Subsequently, the distilled acetate solution needs to be added into the ferric acetylacetonate solution; the mixture solution is stirred at 70 °C for 18 h. Then, a colloidal dispersion is formed by the addition

Table 1
Compilation data obtained for the magnetic properties, fabrication methods and phase analysis of the rare earth substituted (Ba, Sr, Ca and Pb) hexaferrites.

ID	Chemical formula	Method	Sintering (°C, h)	Particle size (nm)	M_S (emu/g)	M_r (emu/g)	H_C(Oe)	(M_r/M_S)	BH_{max} (MGOe)	Phases	Year	Ref.
	Barium hexaferrite											
1	$BaFe_{12}O_{19}$	CP	900	46	44.15	23.68	4930	0.54	-	M-Ba>Fe_2O_3	2015	[26]
2	$BaFe_{12}O_{19}$	SS	1250	1500	67.13	42.42	3206	0.63	-	M-Ba	2017	[28]
3	$BaFe_{12}O_{19}$	CT-SG	800	83	56.90	28.54	4477	0.5	-	M-Ba	2020	[30]
4	$BaFe_{12}O_{19}$	CT-SG	900, 2	86	35.92	18.10	3992	0.5	-	M-Ba	2021	[31]
5	$BaFe_{12}O_{19}$	P-SG	1000, 2	280	56.96	25.6	3828	0.47	-	M-Ba>$BaFeO_3$	2022	[32]
6	$BaFe_{12}O_{19}$	SG-AC	1000	67-370	69.91	44.09	4799	0.63	-	M-Ba	2022	[52]
7	$BaFe_{12}O_{19}$	CT-SG	850	39	68.21	33.60	3200	0.49	-	M-Ba	2022	[53]
8	$BaFe_{12}O_{19}$	ANM	1000, 2	100-250	57.72	31.85	5069	0.55	-	M-Ba>Fe_2O_3	2011	[34]
	Barium hexaferrite substituted with lanthanum											
9	$Ba_{0.9}La_{0.1}Fe_{12}O_{19}$	SS	1250, 3	1344	64.22	41.02	1826	0.64	-	M-Ba	2017	[28]
10	$Ba_{0.8}La_{0.2}Fe_{12}O_{19}$	SS	1250, 3	1568	59.88	38.29	1984	0.64	-	M-Ba	2017	[28]
11	$Ba_{0.9}La_{0.1}Fe_{12}O_{19}$	SS	1100, 2	~3000	11.85	2.67	515	0.22	-	M-Ba	2019	[54] *a
12	$Ba_{0.8}La_{0.2}Fe_{12}O_{19}$	SS	1100, 2	~3000	10.16	2.18	526	0.21	-	M-Ba	2019	[54] *a
13	$Ba_{0.7}La_{0.3}Fe_{12}O_{19}$	SS	1100, 2	~3000	8.73	1.92	505	0.22	-	M-Ba	2019	[54] *a
14	$Ba_{0.6}La_{0.4}Fe_{12}O_{19}$	SS	1100, 2	~3000	6.64	1.34	517	0.20	-	M-Ba	2019	[54] *a
15	$Ba_{0.5}La_{0.5}Fe_{12}O_{19}$	SS	1100, 2	~3000	6.24	1.51	590	0.24	-	M-Ba>Fe_2O_3	2019	[54] *a
16	$Ba_{0.95}La_{0.05}Fe_{12}O_{19}$	CT-SG	1200, 2	~350	57.01	30.40	5141	0.53	-	M-Ba	2019	[55]
17	$Ba_{0.9}La_{0.1}Fe_{12}O_{19}$	CT-SG	1200, 2	~350	63.99	33.83	4684	0.53	-	M-Ba	2019	[55]
18	$Ba_{0.85}La_{0.15}Fe_{12}O_{19}$	CT-SG	1200, 2	~350	53.59	28.14	4745	0.52	-	M-Ba	2019	[55]
19	$Ba_{0.8}La_{0.2}Fe_{12}O_{19}$	CT-SG	1200, 2	~350	45.39	24.42	5622	0.54	-	M-Ba	2019	[55]
20	$Ba_{0.8}La_{0.2}Fe_{12}O_{19}$	SS	1200, 2	~1000	-	-	2809	0.60	-	M-Ba>Fe_2O_3	2019	[29] *b
21	$Ba_{0.6}La_{0.4}Fe_{12}O_{19}$	SS	1200, 2	~1000	-	-	3142	0.62	-	M-Ba>Fe_2O_3, $LaFeO_3$	2019	[29] *b
22	$Ba_{0.4}La_{0.6}Fe_{12}O_{19}$	SS	1200, 2	~1000	-	-	3476	0.64	-	M-Ba>Fe_2O_3, $LaFeO_3$	2019	[29] *b
23	$BaLa_{0.1}Fe_{11.9}O_{19}$	SS	1100, 2	> 500	0.497	0.206	2642	0.41	-	M-Ba	2021	[56] *c
24	$BaLa_{0.2}Fe_{11.8}O_{19}$	SS	1100, 2	> 500	74.60	82.50	1755	1.10	-	M-Ba	2021	[56] *c
25	$BaLa_{0.3}Fe_{11.7}O_{19}$	SS	1100, 2	> 500	54.48	30.32	2293	0.40	-	M-Ba	2021	[56] *c
26	$BaLa_{0.4}Fe_{11.6}O_{19}$	SS	1100, 2	> 500	82.20	43.80	1212	0.53	-	M-Ba	2021	[56] *c
27	$BaLa_{0.5}Fe_{11.5}O_{19}$	SS	1100, 2	> 500	98.10	53.5	3957	0.54	-	M-Ba	2021	[56] *c
28	$BaLa_{0.6}Fe_{11.4}O_{19}$	SS	1100, 2	> 500	52.10	27.07	1710	0.51	-	M-Ba	2021	[56] *c
29	$BaLa_{0.2}Fe_{11.8}O_{19}$	SG	850, 3	57	57.85	32.14	5041	0.55	-	M-Ba	2023	[35]
30	$BaLa_{0.4}Fe_{11.6}O_{19}$	SG	850, 3	53	51.97	28.79	5138	0.55	-	M-Ba	2023	[35]
31	$BaLa_{0.6}Fe_{11.4}O_{19}$	SG	850, 3	46	50.86	28.31	5112	0.55	-	M-Ba	2023	[35]
32	$BaLa_{0.8}Fe_{11.2}O_{19}$	SG	850, 3	44	48.79	27.01	5131	0.55	-	M-Ba	2023	[35]
33	$BaLa_{1.0}Fe_{11.0}O_{19}$	SG	850, 3	39	49.27	27.20	5133	0.55	-	M-Ba	2023	[35]
34	$Ba_{0.9}La_{0.1}Fe_{12}O_{19}$	ANM	1000, 2	100-250	52.09	28.87	5310	0.55	-	M-Ba>Fe_2O_3	2011	[34]
35	$Ba_{0.8}La_{0.2}Fe_{12}O_{19}$	ANM	1000, 2	100-250	50.78	28.12	5424	0.55	-	M-Ba>Fe_2O_3	2011	[34]
36	$Ba_{0.7}La_{0.3}Fe_{12}O_{19}$	ANM	1000, 2	100-250	40.51	22.87	5563	0.56	-	M-Ba>Fe_2O_3	2011	[34]
37	$Ba_{0.6}La_{0.4}Fe_{12}O_{19}$	ANM	1000, 2	100-250	39.99	22.12	5538	0.55	-	M-Ba>Fe_2O_3	2011	[34]
38	$Ba_{0.4}La_{0.6}Fe_{12}O_{19}$	ANM	1000, 2	100-250	16.25	8.62	5284	0.53	-	M-Ba>Fe_2O_3, $LaFeO_3$	2011	[34]
39	$Ba_{0.2}La_{0.8}Fe_{12}O_{19}$	ANM	1000, 2	100-250	17.63	9.37	5246	0.53	-	M-Ba>Fe_2O_3, $LaFeO_3$	2011	[34]
40	$Ba_{0.98}La_{0.02}Fe_{12}O_{19}$	SS	1200, 5	-	60.00	38.23	3232	0.63	-	M-Ba	2019	[57]
41	$Ba_{0.96}La_{0.04}Fe_{12}O_{19}$	SS	1200, 5	-	79.41	50.58	3585	0.63	-	M-Ba	2019	57]
42	$Ba_{0.92}La_{0.08}Fe_{12}O_{19}$	SS	1200, 5	-	39.41	24.11	4343	0.61	-	M-Ba	2019	57]
43	$Ba_{0.9}La_{0.1}Fe_{12}O_{19}$	SS	1250, 3	-	59.10	38.14	2700	0.64	-	-	2014	[58]
44	$Ba_{0.8}La_{0.2}Fe_{12}O_{19}$	SS	1250, 3	-	46.50	23.83	2400	0.51	-	M-Ba>Fe_2O_3	2014	[58]
45	$Ba_{0.9}La_{0.1}Fe_{12}O_{19}$	SS	1250, 3	-	67.50	43.20	2500	0.64	-	-	2014	[58]
46	$Ba_{0.8}La_{0.2}Fe_{12}O_{19}$	SS	1250, 3	-	55.30	34.13	2300	0.62	-	M-Ba>Fe_2O_3	2014	[58]
	Barium hexaferrite substituted with cerium											
47	$BaCe_{0.2}Fe_{11.8}0_{19}$	SG-AC	1100, 4	400-500	49.85	25.00	3518	0.50	-	M-Ba>CeO_2	2015	[36]
48	$BaCe_{0.8}Fe_{11.2}0_{19}$	SG-AC	1100, 4	400-500	56.68	29.66	3357	0.52	-	M-Ba>CeO_2	2015	[36]
49	$Ba_{0.75}Ce_{0.25}Fe_{12}O_{19}$	SS	1100, 2	~1000	44.00	22.23	1779	0.50	-	M-Ba	2019	[59]
50	$Ba_{0.5}Ce_{0.5}Fe_{12}O_{19}$	SS	1100, 2	~1000	13.90	7.51	1782	0.54	-	M-Ba	2019	[59]
51	$Ba_{0.25}Ce_{0.75}Fe_{12}O_{19}$	SS	1100, 2	~1000	10.30	5.12	1767	0.50	-	M-Ba	2019	[59]
52	$Ba_{0.95}Ce_{0.05}Fe_{12}O_{19}$	SG	1100, 3	~500	52.22	28.17	4126	0.54	-	M-Ba	2016	[60]
53	$Ba_{0.9}Ce_{0.1}Fe_{12}O_{19}$	SG	1100, 3	350-500	52.57	28.95	5077	0.55	-	M-Ba	2016	[60]
54	$Ba_{0.85}Ce_{0.15}Fe_{12}O_{19}$	SG	1100, 3	350-500	51.89	27.98	4754	0.54	-	M-Ba>Fe_2O_3	2016	[60]
55	$Ba_{0.8}Ce_{0.2}Fe_{12}O_{19}$	SG	1100, 3	350	47.33	26.24	4710	0.55	-	M-Ba>Fe_2O_3	2016	[60]

(*continued on next page*)

Table 1 (*continued*)

ID	Chemical formula	Method	Sintering (°C, h)	Particle size (nm)	M_S (emu/g)	M_r (emu/g)	H_C(Oe)	(M_r/M_S)	BH_{max} (MGOe)	Phases	Year	Ref.
	Barium hexaferrite substituted with praseodymium											
56	$Ba_{0.95}Pr_{0.05}Fe_{12}O_{19}$	OOPS	1200, 2	1200-1500	27.95	17.04	2055	0.61	-	M-Ba<Fe_2O_3	2014	[37]
57	$Ba_{0.9}Pr_{0.1}Fe_{12}O_{19}$	OOPS	1200, 2	1200-1500	47.05	30.45	3255	0.65	-	M-Ba≈Fe_2O_3	2014	[37]
58	$Ba_{0.85}Pr_{0.15}Fe_{12}O_{19}$	OOPS	1200, 2	1200-1500	49.54	32.05	3372	0.65	-	M-Ba>Fe_2O_3	2014	[37]
59	$Ba_{0.8}Pr_{0.2}Fe_{12}O_{19}$	OOPS	1200, 2	1200-1500	34.10	22.27	3720	0.65	-	M-Ba≈Fe_2O_3	2014	[37]
60	$BaPr_{0.25}Fe_{11.75}O_{19}$	SG	800, 4	10	24.68	13.44	2658	0.54	-	M-Ba	2022	[61]
61	$BaPr_{0.5}Fe_{11.\ 5}O_{19}$	SG	800, 4	6	33.84	18.53	2658	0.54	-	M-Ba	2022	[61]
62	$BaPr_{0.75}Fe_{11.25}O_{19}$	SG	800, 4	7	6.06	0. 73	656	0.12	-	M-Ba	2022	[61]
63	$BaPr_1Fe_{11}O_{19}$	SG	800, 4	6	67.95	37.41	2658	0.55	-	M-Ba	2022	[61]
	Barium hexaferrite substituted with neodymium											
64	$BaFe_{11.75}Nd_{0.25}O_{19}$	CT-SG	850, 2	76	58.24	29.02	4290	0.50	-	M-Ba	2020	[30]
65	$BaFe_{11.5}Nd_{0.5}O_{19}$	CT-SG	850, 2	75	48.47	23.70	3086	0.49	-	M-Ba>Fe_2O_3	2020	[30] *d
66	$BaFe_{11.25}Nd_{0.75}O_{19}$	CT-SG	850, 2	67	49.81	24.86	5234	0.50	-	M-Ba	2020	[30] *d
67	$BaFe_{11}NdO_{19}$	CT-SG	850, 2	65	43.11	21.41	4819	0.50	-	M-Ba	2020	[30] *d
68	$BaNd_{0.02}Fe_{11.98}O_{19}$	SG-AC	-	~655	34.28	11.96	410	0.34	-	M-Ba>Nd_2O_3	2020	[62]
69	$BaNd_{0.04}Fe_{11.96}O_{19}$	SG-AC	-	~655	29.64	10.17	410	0.34	-	M-Ba>Nd_2O_3	2020	[62]
70	$BaNd_{0.06}Fe_{11.94}O_{19}$	SG-AC	-	~655	16.42	5.53	410	0.33	-	M-Ba>Nd_2O_3	2020	[62]
71	$BaNd_{0.1}Fe_{11.9}O_{19}$	HEM	950, 3	-	70.86	38.77	4044	0.54	-	M-Ba>?	2016	[38] *e
72	$BaNd_{0.2}Fe_{11.8}O_{19}$	HEM	950, 3	-	69.61	37.25	4045	0.53	-	M-Ba>?	2016	[38] *e
73	$BaNd_{0.3}Fe_{11.7}O_{19}$	HEM	950, 3	-	74.50	40.91	3113	0.55	-	M-Ba>?	2016	[38] *e
74	$BaNd_{0.1}Fe_{11.9}O_{19}$	HEM	1050, 3	500-1000	81.63	44.21	898	0.54	-	M-Ba>?	2016	[38] *e
75	$BaNd_{0.2}Fe_{11.8}O_{19}$	HEM	1050, 3	500-1000	65.95	34.80	2678	0.53	-	M-Ba>?	2016	[38] *e
76	$BaNd_{0.3}Fe_{11.7}O_{19}$	HEM	1050, 3	~1000	69.00	36.64	610	0.53	-	M-Ba>?	2016	[38] *e
77	$BaFe_{12}O_{19}$, 0.5% Nd_2O_3	SS	1150, 1	-	62.00	36.00	3000	0.58	-	M-Ba	2019	[63] *f
78	$BaFe_{12}O_{19}$, 1.0% Nd_2O_3	SS	1150, 1	-	68.00	30.00	2200	0.44	-	M-Ba	2019	[63] *f
	Barium hexaferrite substituted with samarium											
79	$BaFe_{11.75}Sm_{0.25}O_{19}$	CT-SG	850, 2	38	56.54	21.79	1196	0.47	-	M-Ba	2021	[64]
80	$BaFe_{11.5}Sm_{0.5}O_{19}$	CT-SG	850, 2	46	51.75	23.92	1595	0.46	-	M-Ba>Fe_2O_3, $SmFeO_3$	2021	[64]
81	$BaFe_{11.25}Sm_{0.75}O_{19}$	CT-SG	850, 2	57	60.89	25.90	1649	0.42	-	M-Ba>Fe_2O_3, $SmFeO_3$	2021	[64] *g
82	$BaFe_{11}Sm_1O_{19}$	CT-SG	850, 2	69	63.05	29.26	2265	0.46	-	M-Ba>Fe_2O_3	2021	[64] *g
83	$Ba_{0.98}Sm_{0.02}Fe_{12}O_{19}$	SS-HEM	1250, 2	1040	72.46	33.86	2824	0.48	-	M-Ba	2024	[65]
84	$Ba_{0.96}Sm_{0.04}Fe_{12}O_{19}$	SS-HEM	1250, 2	890	72.32	33.50	2984	0.46	-	M-Ba	2024	[65]
85	$Ba_{0.94}Sm_{0.06}Fe_{12}O_{19}$	SS-HEM	1250, 2	870	73.11	35.22	3096	0.48	-	M-Ba	2024	[65]
86	$Ba_{0.92}Sm_{0.08}Fe_{12}O_{19}$	SS-HEM	1250, 2	1070	72.43	33.32	2936	0.46	-	M-Ba	2024	[65]
87	$Ba_{0.9}Sm_{0.1}Fe_{12}O_{19}$	SS-HEM	1250, 2	1210	68.95	32.19	2840	0.47	-	M-Ba>Fe_2O_3	2024	[65]
	Barium hexaferrite substituted with europium											
88	$Ba_{0.9}Eu_{0.1}Fe_{12}O_{19}$	SG	1100, 2	71	57.46	37.26	2440	0.65	-	M-Ba	2012	[66]
89	$Ba_{0.8}Eu_{0.2}Fe_{12}O_{19}$	SG	1100, 2	73	52.36	35.29	4810	0.67	-	M-Ba	2012	[66]
90	$Ba_{0.75}Eu_{0.25}Fe_{12}O_{19}$	SG	1100, 2	74	45.14	34.52	6120	0.76	-	M-Ba>Fe_2O_3	2012	[66]
91	$Ba_{0.98}Eu_{0.02}Fe_{12}O_{19}$	HT	900, 2	50	34.92	24.17	4172	0.69	-	M-Ba	2017	[39]
92	$Ba_{0.96}Eu_{0.04}Fe_{12}O_{19}$	HT	900, 2	61	43.52	31.34	7146	0.72	-	M-Ba	2017	[39]
93	$Ba_{0.92}Eu_{0.08}Fe_{12}O_{19}$	HT	900, 2	65	56.06	35.64	9352	0.63	-	M-Ba	2017	[39]
	Barium hexaferrite substituted with gadolinium											
94	$Ba_{0.95}Gd_{0.05}Fe_{12}O_{19}$	SG-AC	1000, 3	<180	50.67	31.67	4876	0.62	-	M-Ba>Fe_2O_3	2022	[52]
95	$Ba_{0.90}Gd_{0.10}Fe_{12}O_{19}$	SG-AC	1000, 3	<180	56.14	35.19	4886	0.62	-	M-Ba>Fe_2O_3	2022	[52]
96	$Ba_{0.85}Gd_{0.15}Fe_{12}O_{19}$	SG-AC	1000, 3	<180	47.87	29.85	4945	0.62	-	M-Ba>Fe_2O_3	2022	[52]
97	$Ba_{0.80}Gd_{0.20}Fe_{12}O_{19}$	SG-AC	1000, 3	<180	45.64	28.49	5109	0.62	-	M-Ba>Fe_2O_3	2022	[52]
98	$Ba_{0.75}Gd_{0.25}Fe_{12}O_{19}$	SG-AC	1000, 3	<180	45.04	27.89	5085	0.61	-	M-Ba>Fe_2O_3	2022	[52]
99	$Ba_{0.95}Gd_{0.05}Fe_{12}O_{19}$	SG-AC	1100, 3	<180	45.79	28.17	4933	0.61	-	M-Ba	2022	[52]
100	$Ba_{0.85}Gd_{0.15}Fe_{12}O_{19}$	SG-AC	1100, 3	>180	52.22	32.38	4923	0.6	-	M-Ba>Fe_2O_3	2022	[52]
101	$Ba_{0.75}Gd_{0.25}Fe_{12}O_{19}$	SG-AC	1100, 3	<180	40.28	24.26	4580	0.	-	M-Ba>Fe_2O_3	2022	[52]
102	$BaFe_{11.75}Gd_{0.25}O_{19}$	CT-SG	900, 2	79	49.23	21.90	4727	0.44	-	M-Ba	2021	[31]
103	$BaFe_{11.5}Gd_{0.5}O_{19}$	CT-SG	900, 2	66	54.87	22.30	4875	0.41	-	M-Ba>Fe_2O_3	2021	[31] *h
104	$BaFe_{11.25}Gd_{0.75}O_{19}$	CT-SG	900, 2	53	59.08	23.70	5243	0.40	-	M-Ba>Fe_2O_3	2021	[31] *h
105	$BaFe_{11}GdO_{19}$	CT-SG	900, 2	44	63.64	25.10	5832	0.39	-	M-Ba>Fe_2O_3	2021	[31] *h
106	$Ba_{0.95}Gd_{0.05}Fe_{12}O_{19}$	P-SG	1000, 2	259	55.45	21.50	2911	0.38	-	M-Ba	2022	[32]
107	$Ba_{0.9}Gd_{0.1}Fe_{12}O_{19}$	P-SG	1000, 2	253	51.15	18.95	2896	0.37	-	M-Ba>Fe_2O_3, $GdFeO_3$	2022	[32]
108	$Ba_{0.85}Gd_{0.15}Fe_{12}O_{19}$	P-SG	1000, 2	250	55.55	22.70	3650	0.41	-	M-Ba>Fe_2O_3, $GdFeO_3$	2022	[32]

(*continued on next page*)

Table 1 (*continued*)

ID	Chemical formula	Method	Sintering (°C, h)	Particle size (nm)	M_S (emu/g)	M_r (emu/g)	H_C(Oe)	(M_r/M_S)	BH_{max} (MGOe)	Phases	Year	Ref.
109	$Ba_{0.9}Gd_{0.1}Fe_{12}O_{19}$	SS	1250, 3	1340	64.22	41.03	1826	0.64	-	M-Ba	2017	[28]
110	$Ba_{0.8}Gd_{0.2}Fe_{12}O_{19}$	SS	1250, 3	1560	59.88	38.29	1984	0.64	-	M-Ba	2017	[28]
111	$BaFe_{11.9}Gd_{0.1}O_{19}$	CT-SG	850, 5	38	64.23	31.60	4200	0.49	0.88	M-Ba	2022	[53]
112	$BaFe_{11.7}Gd_{0.3}O_{19}$	CT-SG	850, 5	36	63.38	30.80	4300	0.49	0.85	M-Ba	2022	[53]
113	$BaFe_{11.5}Gd_{0.5}O_{19}$	CT-SG	850,5	33	57.73	28.10	4500	0.49	0.72	M-Ba	2022	[53]
114	$BaFe_{11.3}Gd_{0.7}O_{19}$	CT-SG	850, 5	29	54.23	26.30	4800	0.48	0.64	M-Ba	2022	[53]
115	$Ba_{0.9}Gd_{0.1}Fe_{12}O_{19}$	SS	1200, 3	2070	51.77	29.8	1723	0.58	-	M-Ba	2023	[67]
116	$Ba_{0.875}Gd_{0.125}Fe_{12}O_{19}$	SS	1200, 3	2360	55.66	32.40	1593	0.58	-	M-Ba	2023	[67]
117	$Ba_{0.85}Gd_{0.15}Fe_{12}O_{19}$	SS	1200, 3	2620	48.38	27.76	1662	0.57	-	M-Ba>Fe_2O_3	2023	[67]
118	$Ba_{0.8}Gd_{0.2}Fe_{12}O_{19}$	SS	1200, 3	1970	46.89	28.23	1832	0.60	-	M-Ba>Fe_2O_3	2023	[67]
119	$Ba_{0.5}Gd_{0.5}Fe_{12}O_{19}$	SS	1200, 3	1860	29.48	17.77	1919	0.60	-	M-Ba>Fe_2O_3	2023	[67]
	Barium hexaferrite substituted with holmium											
120	$BaFe_{11.8}Ho_{0.2}O_{19}$	SS	1275, 1	2600	15.01	8.70	2201	0.58	-	M-Ba>Fe_2O_3, Ho_2O_3	2010	[68]
121	$BaFe_{11.6}Ho_{0.4}O_{19}$	SS	1275, 1	1810	52.59	29.07	2230	0.55	-	M-Ba>Fe_2O_3, $Ho_3Fe_5O_{12}$	2010	[68]
122	$BaFe_{11.4}Ho_{0.6}O_{19}$	SS	1275, 1	1670	23.04	12.54	1889	0.54	-	M-Ba>Fe_2O_3, $Ho_3Fe_5O_{12}$	2010	[68]
123	$BaFe_{11.2}Ho_{0.8}O_{19}$	SS	1275, 1	1210	16.95	9.10	1910	0.53	-	M-Ba>Fe_2O_3, $Ho_3Fe_5O_{12}$	2010	[68]
124	$BaFe_{11}Ho_1O_{19}$	SS	1275, 1	2140	13.34	7.06	1951	0.53	-	M-Ba>Ho_2O_3	2010	[68]
	Strontium hexaferrite											
125	$SrFe_{12}O_{19}$	CT-SG	950, 3	70-80	60.00	30.15	6117	0.5	-	M-Sr>Fe_2O_3	2016	[69]
126	$SrFe_{12}O_{19}$	SG-AC	1000, 3	45	66.25	40.91	8972	0.62	-	M-Sr	2022	[70]
127	$SrFe_{12}O_{19}$	SG-PC	1050, 2	86	60.46	32.14	5540	0.53	0.77	M-Sr	2023	[40]
128	$SrFe_{12}O_{19}$	CT-SG	750, 2	5.8	40.91	29.8	2550	0.73	-	M-Sr>Fe_2O_3	2021	[71]
129	$SrFe_{12}O_{19}$	CT-SG	1100, 5	77	68.56	34.74	4337	0.51	-	M-Sr	2018	[72]
130	$SrFe_{12}O_{19}$	SG-PC	1100, 4	1500	72.23	33.45	2000	0.46	0.67	M-Sr	2024	[73]
131	$SrFe_{12}O_{19}$	SG	1100, 3	0.54	65.92	49.65	5957	0.75	-	M-Sr	2016	[42]
132	$SrFe_{12}O_{19}$	SG-AC	1100, 6	35.9	69.00	35.00	4300	0.50	-	M-Sr>Fe_2O_3	2021	[74]
133	$SrFe_{12}O_{19}$	SG	1300, 2	2135	58.83	30.40	1318	0.51	-	M-Sr	2018	[75]
134	$SrFe_{12}O_{19}$	SS	1250, 2	2500	84.00	32.00	1800	0.38	-	M-Sr	2020	[76]
135	$SrFe_{12}O_{19}$	SS	1280, 2	3000	60.80	11.63	2430	0.19	0.67	M-Sr	2019	[77]
136	$SrFe_{12}O_{19}$	HT	1100, 1	92	51.98	22.04	1114	0.42	-	M-Sr	2019	[78]
137	$SrFe_{12}O_{19}$	TP	1200, 2	5000	60.07	16.04	1100	0.26	-	M-Sr	2020	[41]
	Strontium hexaferrite substituted with lanthanum											
138	$Sr_{0.975}La_{0.025}Fe_{12}O_{19}$	SG-PC	1100, 4	200-300	71.72	32.50	5070	0.45	0.94	M-Sr	2024	[73]
139	$Sr_{0.95}La_{0.05}Fe_{12}O_{19}$	SG-PC	1100, 4	200-300	72.10	32.53	4630	0.45	0.92	M-Sr	2024	[73]
140	$Sr_{0.925}La_{0.075}Fe_{12}O_{19}$	SG-PC	1100, 4	200-300	66.31	29.87	4530	0.45	0.78	M-Sr	2024	[73]
141	$Sr_{0.9}La_{0.1}Fe_{12}O_{19}$	SG-PC	1100, 4	200-300	74.25	34.09	1960	0.45	0.68	M-Sr	2024	[73]
142	$Sr_{0.95}La_{0.05}Fe_{12}O_{19}$	MS-SG	1100, 3	440	67.35	50.93	6119	0.76	-	M-Sr	2016	[42]
143	$Sr_{0.90}La_{0.1}Fe_{12}O_{19}$	MS-SG	1100, 3	420	68.77	48.78	6105	0.71	-	M-Sr	2016	[42]
144	$Sr_{0.85}La_{0.15}Fe_{12}O_{19}$	MS-SG	1100, 3	360	69.52	49.53	6252	0.71	-	M-Sr	2016	[42]
145	$Sr_{0.80}La_{0.2}Fe_{12}O_{19}$	MS-SG	1100, 3	340	67.46	48.58	6021	0.72	-	M-Sr	2016	[42]
146	$Sr_{0.92}La_{0.08}Fe_{12}O_{19}$	CT-SG	950, 3	33	55.89	33.20	6110	0.59	-	M-Sr	2015	[79]
147	$Sr_{0.87}La_{0.13}Fe_{12}O_{19}$	CT-SG	950, 3	31	53.81	31.33	6960	0.58	-	M-Sr	2015	[79]
148	$Sr_{0.82}La_{0.18}F_{12}O_{19}$	CT-SG	950, 3	29	52.40	30.50	7060	0.58	-	M-Sr	2015	[79]
149	$SrLa_{0.23}Fe_{11.77}O_{19}$	CT-SG	900, 4	-	47.40	-	6201	-	-	M-Sr	2013	[80]
150	$SrLa_{0.43}Fe_{11.57}O_{19}$	CT-SG	900, 4	-	45.33	-	6230	-	-	M-Sr	2013	[80]
151	$SrLa_{0.63}Fe_{11.37}O_{19}$	CT-SG	900, 4	-	41.17	-	6326	-	-	M-Sr	2013	[80]
152	$SrLa_{0.83}Fe_{11.17}O_{19}$	CT-SG	900, 4	~500	36.82	-	6207	-	-	M-Sr	2013	[80]
153	$SrLa_1Fe_{11}O_{19}$	CT-SG	900, 4	~100	32.46	-	5831	-	-	M-Sr	2013	[80]
154	$Sr_{0.9}La_{0.1}Fe_{12}O_{19}$	SPS	950, 0.1		42.83	22.45	3170	0.52	-	M-Sr	2021	[43]
155	$Sr_{07}La_{0.3}Fe_{12}O_{19}$	SPS	950, 0.1		30.75	16.03	3170	0.52	-	M-Sr	2021	[43]
156	$Sr_{0.4}La_{0.6}Fe_{12}O_{19}$	SPS	950, 0.1		26.98	13.39	2915	0.49	-	M-Sr	2021	[43]
157	$Sr_{0.8}La_{0.2}Fe_{12}O_{19}$	SS	1150, 1	400	87.00	54.00	4796	0.62	-	M-Sr>Fe_2O_3	2012	[81]
158	$Sr_{0.8}La_{0.2}Fe_{12}O_{19}$	SS	1200, 1	600	96.00	60.00	4510	0.63	-	M-Sr>Fe_2O_3	2012	[81]
159	$Sr_{0.8}La_{0.2}Fe_{12}O_{19}$	SS	1250, 1	1200	67.00	59.00	3847	0.88	-	M-Sr>Fe_2O_3	2012	[81]
160	$Sr_{0.8}La_{0.2}Fe_{12}O_{19}$	SS	1300, 1	2110	102.00	56.00	1781	0.55	-	M-Sr	2012	[81]
161	$Sr_{0.9}La_{0.1}Fe_{12}O_{19}$	SG-AC	900, 2	~1000	59.6	29.8	5046	0.50	0.65	M-Sr>Fe_2O_3	2019	[82]
162	$Sr_{0.9}La_{0.1}Fe_{12}O_{19}$	SG-AC	1100, 2	200–350	62.3	31.3	5046	0.50	0.71	M-Sr>Fe_2O_3	2019	[82]
163	$Sr_{0.9}La_{0.1}Fe_{12}O_{19}$	SG-AC	1200, 2	~100	62.7	35.3	4006	0.56	0.94	M-Sr>Fe_2O_3	2019	[82]
	Strontium hexaferrite substituted with cerium											
164	$SrCe_{0.03}Fe_{11.97}O_{19}$	SG-AC	1050, 2.5	290-40	61.83	35.09	5902	0.56	-	M-Sr>CeO_2	2020	[83]
165	$SrCe_{0.05}Fe_{11.95}O_{19}$	SG-AC	1050, 2.5	290-40	52.49	35.86	6152	0.57	-	M-Sr> Fe_2O_3, CeO_2	2020	[83]
166	$SrCe_{0.07}Fe_{11.93}O_{19}$	SG-AC	1050, 2.5	290-40	71.17	30.08	5530	0.56	-	M-Sr>CeO_2	2020	[83]
167	$SrCe_{0.1}Fe_{11.9}O_{19}$	SG-AC	1050, 2.5	290-40	45.72	40.12	5227	0.55	-	M-Sr>CeO_2	2020	[83]
168	$Sr_{0.99}Ce_{0.01}Fe_{12}O_{19}$	AC	1100, 3	70-95	66.44	39.59	9682	0.61	-	M-Sr	2022	[44]
169	$Sr_{0.95}Ce_{0.05}Fe_{12}O_{19}$	AC	1100, 3	70-95	47.73	29.63	9351	0.62	-	M-Sr	2022	[44]
170	$Sr_{0.91}Ce_{0.09}Fe_{12}O_{19}$	AC	1100, 3	70-95	43.62	26.12	8274	0.62	-	M-Sr> Fe_2O_3	2022	[44]
171	$Sr_{0.97}Ce_{0.03}Fe_{12}O_{19}$	SG-AC	1200, 3	~650	77.73	38.04	4483	0.49	-	M-Sr	2024	[84]
172	$Sr_{0.95}Ce_{0.05}Fe_{12}O_{19}$	SG-AC	1200, 3	~810	74.53	36.73	4468	0.49	-	M-Sr	2024	[84]
173	$Sr_{0.9}Ce_{0.1}Fe_{12}O_{19}$	SG-AC	1200, 3	~750	71.12	35.08	4491	0.49	-	M-Sr>Fe_2O_3, CeO_2	2024	[84]
174	$Sr_{0.8}Ce_{0.2}Fe_{12}O_{19}$	SG-AC	1200, 3	~710	62.60	30.86	4638	0.49	-	M-Sr>Fe_2O_3, CeO_2	2024	[84]
175	$SrCe_{0.1}Fe_{11.9}O_{19}$	CT-SG	1100, 5	67	58.45	29.82	3733	0.51	-	M-Sr	2018	[72]

(*continued on next page*)

Table 1 (*continued*)

ID	Chemical formula	Method	Sintering (°C, h)	Particle size (nm)	M_S (emu/g)	M_r (emu/g)	H_C(Oe)	(M_r/M_S)	BH_{max} (MGOe)	Phases	Year	Ref.
176	$SrCe_{0.2}Fe_{11.8}O_{19}$	CT-SG	1100, 5	65	53.12	26.14	3777	0.51	-	M-Sr	2018	[72]
177	$SrCe_{0.3}Fe_{11.7}O_{19}$	CT-SG	1100, 5	48	51.24	25.52	4222	0.49	-	M-Sr	2018	[72]
178	$SrCe_{0.4}Fe_{11.6}O_{19}$	CT-SG	1100, 5	64	47.41	23.68	4300	0.49	-	M-Sr>Fe_2O_3	2018	[72]
179	$SrCe_{0.5}Fe_{11.5}O_{19}$	CT-SG	1100, 5	51	46.69	23.27	4522	0.49	-	M-Sr>Fe_2O_3	2018	[72]
180	$Sr_{0.95}Ce_{0.05}Fe_{12}O_{19}$	SG	900, 2	-	56.35	29.97	1375	0.54	-	M-Sr	2018	[75]
181	$Sr_{0.85}Ce_{0.15}Fe_{12}O_{19}$	SG	900, 2	-	5.83	23.20	515	0.51	-	M-Sr>Fe_2O_3	2018	[75]
182	$Sr_{0.8}Ce_{0.2}Fe_{12}O_{19}$	SG	900, 2	1045	44.67	21.83	1359	0.49	-	M-Sr>Fe_2O_3	2018	[75]
183	$Sr_{0.75}Ce_{0.25}Fe_{12}O_{19}$	SG	900, 2	1776	38.22	20.22	1737	0.53	-	M-Sr>Fe_2O_3, CeO_2	2018	[75]
184	$Sr_{0.9}Ce_{0.1}Fe_{12}O_{19}$	SG-AC	900, 2	~1000	51.5	27.9	4284	0.54	0.96	M-Sr>Fe_2O_3	2019	[82]
185	$Sr_{0.9}Ce_{0.1}Fe_{12}O_{19}$	SG-AC	1100, 2	200–350	59.6	31.7	5388	0.53	0.76	M-Sr>Fe_2O_3	2019	[82]
186	$Sr_{0.9}Ce_{0.1}Fe_{12}O_{19}$	SG-AC	1200, 2	~100	64.3	34.8	6159	0.54	0.59	M-Sr>Fe_2O_3	2019	[82]
187	$Sr_{0.98}Ce_{0.02}Fe_{12}O_{19}$	HEM	1200, 2	1150	73.62	35.35	3878	0.48	-	M-Sr	2024	[85]
188	$Sr_{0.96}Ce_{0.04}Fe_{12}O_{19}$	HEM	1200, 2	1420	72.36	34.74	3750	0.48	-	M-Sr	2024	[85]
189	$Sr_{0.94}Ce_{0.06}Fe_{12}O_{19}$	HEM	1200, 2	1560	70.75	34.87	3766	0.49	-	M-Sr>Fe_2O_3	2024	[85]
190	$Sr_{0.92}Ce_{0.08}Fe_{12}O_{19}$	HEM	1200, 2	1810	70.70	34.38	3559	0.48	-	M-Sr>Fe_2O_3	2024	[85]
191	$Sr_{0.99}Ce_{0.01}Fe_{12}O_{19}$	AC	1100, 20	43	66.14	40.99	9735	0.62	-	M-Sr	2022	[86]
192	$Sr_{0.97}Ce_{0.03}Fe_{12}O_{19}$	AC	1100, 20	42	53.95	33.56	9519	0.62	-	M-Sr	2022	[86]
193	$Sr_{0.95}Ce_{0.05}Fe_{12}O_{19}$	AC	1100, 20	43	47.93	29.75	9642	0.62	-	M-Sr	2022	[86]
194	$Sr_{0.93}Ce_{0.07}Fe_{12}O_{19}$	AC	1100, 20	43	46.08	28.29	9527	0.61	-	M-Sr	2022	[86]
195	$Sr_{0.91}Ce_{0.09}Fe_{12}O_{19}$	AC	1100, 20	42	43.81	27.06	8146	0.62	-	M-Sr>Fe_2O_3	2022	[86]
	Strontium hexaferrite substituted with praseodymium											
196	$SrFe_{11.95}Pr_{0.05}O_{19}$	SG-AC	1100, 3	100-500	72.57	36.91	5069	0.51	-	M-Sr	2023	[87]
197	$SrFe_{11.9}Pr_{0.1}O_{19}$	SG-AC	1100, 3	100-500	65.38	33.51	5459	0.51	-	M-Sr	2023	[87]
198	$SrFe_{11.85}Pr_{0.15}O_{19}$	SG-AC	1100, 3	100-500	68.00	34.80	5469	0.51	-	M-Sr	2023	[87]
199	$SrFe_{11.8}Pr_{0.2}O_{19}$	SG-AC	1100, 3	100-500	67.72	34.25	5620	0.51	-	M-Sr>$FePr_{1-y}Sr_yO_3$	2023	[87]
200	$SrFe_{11.75}Pr_{0.25}O_{19}$	SG-AC	1100, 3	100-500	64.55	32.90	5669	0.51	-	M-Sr>$FePr_{1-y}Sr_yO_3$	2023	[87]
201	$SrFe_{11.7}Pr_{0.3}O_{19}$	SG-AC	1100, 3	100-500	62.70	32.10	5625	0.51	-	M-Sr>$FePr_{1-y}Sr_yO_3$	2023	[87]
202	$SrFe_{11.65}Pr_{0.35}O_{19}$	SG-AC	1100, 3	100-500	62.87	32.09	5665	0.51	-	M-Sr>$FePr_{1-y}Sr_yO_3$	2023	[87]
203	$SrFe_{11.6}Pr_{0.4}O_{19}$	SG-AC	1100, 3	100-500	63.94	32.79	5857	0.51	-	M-Sr>$FePr_{1-y}Sr_yO_3$	2023	[87]
204	$SrFe_{11.55}Pr_{0.45}O_{19}$	SG-AC	1100, 3	100-500	66.56	33.90	5878	0.51	-	M-Sr>$FePr_{1-y}Sr_yO_3$	2023	[87]
205	$SrFe_{11.5}Pr_{0.5}O_{19}$	SG-AC	1100, 3	100-500	65.04	33.18	5870	0.51	-	M-Sr>$FePr_{1-y}Sr_yO_3$	2023	[87]
206	$Sr_{0.975}Pr_{0.025}Fe_{12}O_{19}$	SG-PC	1100, 4	200-400	77.35	33.35	5460	0.43	1.09	M-Sr	2024	[73]
207	$Sr_{0.95}Pr_{0.05}Fe_{12}O_{19}$	SG-PC	1100, 4	200-400	70.52	32.19	5340	0.46	0.92	M-Sr	2024	[73]
208	$Sr_{0.925}Pr_{0.075}Fe_{12}O_{19}$	SG-PC	1100, 4	200-400	73.36	33.38	5350	0.45	0.98	M-Sr	2024	[73]
209	$Sr_{0.9}Pr_{0.1}Fe_{12}O_{19}$	SG-PC	1100, 4	200-400	75.73	34.53	3120	0.46	0.82	M-Sr	2024	[73]
210	$Sr_{0.85}Pr_{0.15}Fe_{12}O_{19}$	SG-MW	800, 1.3	37	64.60	33.90	3835	0.52	-	M-Sr	2014	[45]
211	$Sr_{0.75}Pr_{0.25}Fe_{12}O_{19}$	SG-MW	800, 1.3	36	61.23	32.37	4093	0.52	-	M-Sr>Fe_2O_3	2014	[45]
212	$Sr_{0.5}Pr_{0.5}Fe_{12}O_{19}$	SG-MW	800, 1.3	46	49.88	23.02	1895	0.46	-	M-Sr>Fe_2O_3, $PrFeO_3$	2014	[45]
	Strontium hexaferrite substituted with neodymium											
213	$Sr_{0.95}Nd_{0.05}Fe_{12}O_{19}$	CT-SG	950, 3	70-80	63.00	38.09	6634	0.53	-	M-Sr>Fe_2O_3, Nd_2O_3	2016	[69]
214	$Sr_{0.9}Nd_{0.1}Fe_{12}O_{19}$	CT-SG	950, 3	70-80	65.00	35.52	6704	0.53	-	M-Sr>Fe_2O_3, Nd_2O_3	2016	[69]
215	$Sr_{0.85}Nd_{0.15}Fe_{12}O_{19}$	CT-SG	950, 3	70-80	63.00	35.15	6885	0.53	-	M-Sr>Fe_2O_3, Nd_2O_3	2016	[69]
216	$Sr_{0.8}Nd_{0.2}Fe_{12}O_{19}$	CT-SG	950, 3	70-80	63.00	34.23	6703	0.54	-	M-Sr>Fe_2O_3, Nd_2O_3	2016	[69]
217	$Sr_{0.9}Nd_{0.1}Fe_{12}O_{19}$	SG-PC	900, 2	81	59.88	32.21	6872	0.53	0.76	M-Sr>Fe_2O_3, $NdFeO_3$	2023	[40]
218	$Sr_{0.8}Nd_{0.2}Fe_{12}O_{19}$	SG-PC	900, 2	121	60.3	32.06	6880	0.53	0.80	M-Sr>Fe_2O_3, $NdFeO_3$	2023	[40]
219	$Sr_{0.7}Nd_{0.3}Fe_{12}O_{19}$	SG-PC	900, 2	137	59.8	31.09	6990	0.52	0.85	M-Sr> $NdFeO_3$	2023	[40]
220	$Sr_{0.6}Nd_{0.4}Fe_{12}O_{19}$	SG-PC	900, 2	160	60.40	32.06	6920	0.53	0.90	M-Sr>, $NdFeO_3$	2023	[40]
221	$Sr_{0.9}Nd_{0.1}Fe_{12}O_{19}$	SG-PC	1000, 2	288	61.78	32.64	6257	0.53	1.03	M-Sr>Fe_2O_3, $NdFeO_3$	2023	[40]
222	$Sr_{0.8}Nd_{0.2}Fe_{12}O_{19}$	SG-PC	1000, 2	358	63.13	33.50	6440	0.53	0.91	M-Sr>Fe_2O_3, $NdFeO_3$	2023	[40]
223	$Sr_{0.7}Nd_{0.3}Fe_{12}O_{19}$	SG-PC	1000, 2	364	63.57	33.32	6651	0.52	0.97	M-Sr>Fe_2O_3, $NdFeO_3$	2023	[40]
224	$Sr_{0.6}Nd_{0.4}Fe_{12}O_{19}$	SG-PC	1000, 2	404	61.60	33.00	6147	0.54	0.91	M-Sr>Fe_2O_3, $NdFeO_3$	2023	[40]
225	$Sr_{0.9}Nd_{0.1}Fe_{12}O_{19}$	SG-PC	1050, 2	832	65.69	34.69	6130	0.53	1.04	M-Sr>Fe_2O_3, $NdFeO_3$	2023	[40]
226	$Sr_{0.8}Nd_{0.2}Fe_{12}O_{19}$	SG-PC	1050, 2	958	62.13	32.85	6130	0.53	0.94	M-Sr>Fe_2O_3, $NdFeO_3$	2023	[40]
227	$Sr_{0.7}Nd_{0.3}Fe_{12}O_{19}$	SG-PC	1050, 2	690	62.67	33.04	6420	0.53	0.96	M-Sr>Fe_2O_3, $NdFeO_3$	2023	[40]
228	$Sr_{0.6}Nd_{0.4}Fe_{12}O_{19}$	SG-PC	1050, 2	1122	60.73	31.89	6260	0.53	0.79	M-Sr>Fe_2O_3, $NdFeO_3$	2023	[40]
229	$Sr_{0.9}Nd_{0.1}Fe_{12}O_{19}$	SG-PC	1100, 2	1009	62.65	33.60	5540	0.54	0.94	M-Sr> $NdFeO_3$	2023	[40]
230	$Sr_{0.8}Nd_{0.2}Fe_{12}O_{19}$	SG-PC	1100, 2	1079	63.31	33.56	5820	0.53	0.97	M-Sr>Fe_2O_3, $NdFeO_3$	2023	[40]
231	$Sr_{0.7}Nd_{0.3}Fe_{12}O_{19}$	SG-PC	1100, 2	1062	62.88	33.02	6020	0.53	0.95	M-Sr> $NdFeO_3$	2023	[40]
232	$Sr_{0.6}Nd_{0.4}Fe_{12}O_{19}$	SG-PC	1100, 2	1075	59.81	31.40	6040	0.52	0.87	M-Sr> $NdFeO_3$	2023	[40]
233	$Sr_{0.975}Nd_{0.025}Fe_{12}O_{19}$	SG-PC	1100, 4	250-450	73.74	33.86	4330	0.46	0.97	M-Sr	2024	[73]
234	$Sr_{0.95}Nd_{0.05}Fe_{12}O_{19}$	SG-PC	1100, 4	250-450	70.05	32.32	3860	0.46	0.88	M-Sr	2024	[73]
235	$Sr_{0.925}Nd_{0.075}Fe_{12}O_{19}$	SG-PC	1100, 4	250-450	75.17	34.95	3810	0.46	1.03	M-Sr	2024	[73]
236	$Sr_{0.9}Nd_{0.1}Fe_{12}O_{19}$	SG-PC	1100, 4	250-450	74.37	34.05	2800	0.46	0.80	M-Sr	2024	[73]
237	$Sr_{0.9}Nd_{0.1}Fe_{12}O_{19}$	SG-AC	1000, 1	-	60.60	39.10	5020	0.64	-	M-Sr	2023	[88]
238	$Sr_{0.9}Nd_{0.1}Fe_{12}O_{19}$	SG-AC	1100, 1	-	61.50	40.20	5210	0.65	-	M-Sr	2023	[88]
239	$Sr_{0.9}Nd_{0.1}Fe_{12}O_{19}$	SG-AC	1200, 1	-	59.20	38.90	4420	0.66	-	M-Sr	2023	[88]
240	$Sr_{0.9}Nd_{0.1}Fe_{12}O_{19}$	SS	1100, 5	-	9.07	3.50	1090	0.38	-	M-Sr>$SrFe_6O1_3$	2020	[89]
241	$Sr_{0.8}Nd_{0.2}Fe_{12}O_{19}$	SS	1100, 5	-	5.52	2.29	1090	0.41	-	M-Sr>$SrFe_6O1_3$, $SrNdFeO_4$	2020	[89]
242	$Sr_{0.7}Nd_{0.3}Fe_{12}O_{19}$	SS	1100, 5	-	3.51	1.50	1090	0.53	-	M-Sr>$SrFe_6O1_3$, $SrNdFeO_4$	2020	[89]
243	$SrFe_{11.9}Nd_{0.1}O_{19}$	HEM	1000, 2	65	66.62	34.80	5420	0.52		M-Sr>Fe_2O_3	2022	[90]
244	$SrFe_{11.8}Nd_{0.2}O_{19}$	HEM	1000, 2	68	59.81	31.12	5610	0.52		M-Sr>Fe_2O_3	2022	[90]

(*continued on next page*)

Table 1 (*continued*)

ID	Chemical formula	Method	Sintering (°C, h)	Particle size (nm)	M_S (emu/g)	M_r (emu/g)	H_C(Oe)	(M_r/M_S)	BH_{max} (MGOe)	Phases	Year	Ref.
245	$SrFe_{11.7}Nd_{0.3}O_{19}$	HEM	1000, 2	80	50.14	26.59	5690	0.53	-	M-Sr>Fe_2O_3>$SrFeO_{2.83}$	2022	[90]
246	$SrFe_{11.6}Nd_{0.4}O_{19}$	HEM	1000, 2	86	42.81	22.95	5780	0.54	-	M-Sr~Fe_2O_3>$SrFeO_{2.83}$	2022	[90]
247	$SrFe_{11.5}Nd_{0.5}O_{19}$	HEM	1000, 2	102	35.23	18.51	5610	0.52	-	M-Sr~Fe_2O_3>$SrFeO_{2.83}$	2022	[90]
	Strontium hexaferrite substituted with samarium											
248	$Sr_{0.975}Sm_{0.025}Fe_{12}O_{19}$	SG-PC	1100, 4	230-550	76.50	34.46	5380	0.45	1.03	M-Sr	2024	[73]
249	$Sr_{0.95}Sm_{0.05}Fe_{12}O_{19}$	SG-PC	1100, 4	230-550	71.56	32.36	5320	0.45	0.91	M-Sr	2024	[73]
250	$Sr_{0.925}Sm_{0.075}Fe_{12}O_{19}$	SG-PC	1100, 4	230-550	69.90	31.62	5580	0.45	0.88	M-Sr	2024	[73]
251	$Sr_{0.9}Sm_{0.1}Fe_{12}O_{19}$	SG-PC	1100, 4	230-550	68.71	31.56	3840	0.45	0.80	M-Sr	2024	[73]
252	$SrSm_{0.01}Fe_{11.99}O_{19}$	SCH	1000, 3	301	34.76	20.00	6600	0.57	-	M-Sr>Fe_2O_3	2024	[46]
253	$SrSm_{0.02}Fe_{11.98}O_{19}$	SCH	1000, 3	254	48.52	27.60	5802	0.56	-	M-Sr>Fe_2O_3	2024	[46]
254	$SrSm_{0.03}Fe_{11.97}O_{19}$	SCH	1000, 3	285	53.10	29.40	5790	0.57	-	M-Sr>Fe_2O_3	2024	[46]
255	$SrFe_{11.99}Sm_{0.01}O_{19}$	SG	1200, 4	2120	72.55	45.29	1987	0.55	-	M-Sr	2018	[91]
256	$SrFe_{11.98}Sm_{0.02}O_{19}$	SG	1200, 4	1420	69.89	42.56	1955	0.62	-	M-Sr	2018	[91]
257	$SrFe_{11.97}Sm_{0.03}O_{19}$	SG	1200, 4	1580	71.50	43.84	1871	0.61	-	M-Sr	2018	[91]
258	$SrSm_{0.1}Fe_{11.9}O_{19}$	SG-AC	1200, 2	500-700	61.67	31.25	2858	0.50	-	M-Sr	2024	[92]
259	$SrSm_{0.2}Fe_{11.8}O_{19}$	SG-AC	1200, 2	500-700	54.40	29.40	3320	0.54	-	M-Sr>?	2024	[92][*i]
260	$SrSm_{0.3}Fe_{11.7}O_{19}$	SG-AC	1200, 2	500-700	51.56	27.71	3378	0.53	-	M-Sr>?	2024	[92][*i]
261	$SrSm_{0.4}Fe_{11.6}O_{19}$	SG-AC	1200, 2	500-700	48.76	25.96	3428	0.53	-	M-Sr>?	2024	[92][*i]
262	$SrSm_{0.5}Fe_{11.5}O_{19}$	SG-AC	1200, 2	500-700	44.85	24.65	3495	0.54	-	M-Sr>?	2024	[92][*i]
263	$Sr_{0.95}Sm_{0.05}Fe_{12}O_{19}$	P-SG	1000, 2	~1000	61.71	37.19	~500	0.60	-	M-Sr	2016	[33]
264	$Sr_{0.9}Sm_{0.1}Fe_{12}O_{19}$	P-SG	1000, 2	~1000	60.05	27.22	~500	0.45	-	M-Sr>Fe_2O_3	2016	[33]
265	$Sr_{0.85}Sm_{0.15}Fe_{12}O_{19}$	P-SG	1000, 2	~1000	64.62	32.62	~500	0.50	-	M-Sr>Fe_2O_3	2016	[33]
	Strontium hexaferrite substituted with europium											
266	$Sr_{0.95}Eu_{0.05}Fe_{12}O_{19}$	SS	1250, 3	~2000	78.03	23.91	1014	0.30	-	M-Sr	2020	[93]
267	$Sr_{0.9}Eu_{0.1}Fe_{12}O_{19}$	SS	1250, 3	~2000	78.49	38.26	2850	0.49	-	M-Sr	2020	[93]
268	$Sr_{0.85}Eu_{0.15}Fe_{12}O_{19}$	SS	1250, 3	~2000	81.85	37.39	2680	0.46	-	M-Sr>Fe_2O_3	2020	[93]
269	$Sr_{0.8}Eu_{0.2}Fe_{12}O_{19}$	SS	1250, 3	~2000	81.22	37.82	2800	0.46	-	M-Sr>Fe_2O_3	2020	[93]
270	$Sr_{0.75}Eu_{0.25}Fe_{12}O_{19}$	SS	1250, 3	~2000	65.21	26.95	2700	0.41	-	M-Sr>Fe_2O_3	2020	[93]
	Strontium hexaferrite substituted with gadolinium											
271	$Sr_{0.95}Gd_{0.05}Fe_{12}O_{19}$	SS	1250, 2	~3000	90.00	9.00	220	0.10	-	M-Sr	2020	[76]
272	$Sr_{0.9}Gd_{0.1}Fe_{12}O_{19}$	SS	1250, 2	~3000	78.00	34.00	2800	0.43	-	M-Sr	2020	[76]
273	$Sr_{0.85}Gd_{0.15}Fe_{12}O_{19}$	SS	1250, 2	~3000	73.00	35.00	2900	0.48	-	M-Sr>Fe_2O_3	2020	[76]
274	$Sr_{0.8}Gd_{0.2}Fe_{12}O_{19}$	SS	1250, 2	~3000	72.00	33.00	3075	0.46	-	M-Sr>Fe_2O_3	2020	[76]
275	$Sr_{0.75}Gd_{0.25}Fe_{12}O_{19}$	SS	1250, 2	~3000	64.00	29.00	3230	0.45	-	M-Sr>Fe_2O_3	2020	[76]
276	$SrFe_{11.75}Gd_{0.25}O_{19}$	CT-SG	750, 2	48	57.70	31.90	6099	0.55	-	M-Sr>Fe_2O_3	2021	[71]
277	$SrFe_{11.5}Gd_{0.5}O_{19}$	CT-SG	750, 2	52	53.34	32.50	6195	0.61	-	M-Sr>Fe_2O_3	2021	[71]
278	$SrFe_{11.25}Gd_{0.75}O_{19}$	CT-SG	750, 2	56	54.48	28.20	6310	0.52	-	M-Sr>Fe_2O_3	2021	[71]
279	$SrFe_{11}Gd_1O_{19}$	CT-SG	750, 2	62	42.74	26.30	5912	0.61	-	M-Sr>Fe_2O_3	2021	[71]
280	$Sr_{0.09}Gd_{0.01}Fe_{12}O_{19}$	SG-AC	1100, 3	44	53.95	33.56	8146	0.62	-	M-Sr	2022	[70]
281	$Sr_{0.07}Gd_{0.03}Fe_{12}O_{19}$	SG-AC	1100, 3	41	49.93	29.98	9419	0.60	-	M-Sr	2022	[70]
282	$Sr_{0.05}Gd_{0.05}Fe_{12}O_{19}$	SG-AC	1100, 3	44	45.42	28.03	9513	0.61	-	M-Sr	2022	[70]
283	$Sr_{0.03}Gd_{0.07}Fe_{12}O_{19}$	SG-AC	1100, 3	43	41.65	25.37	9587	0.61	-	M-Sr	2022	[70]
284	$Sr_{0.01}Gd_{0.09}Fe_{12}O_{19}$	SG-AC	1100, 3	43	39.16	24.25	9064	0.62	-	M-Sr>Fe_2O_3	2022	[70]
285	$SrGd_{0.01}Fe_{11.99}O_{19}$	SG-AC	1100, 6	~1000	67.43	36.30	3200	0.54	-	M-Sr	2021	[74]
286	$SrGd_{0.02}Fe_{11.98}O_{19}$	SG-AC	1100, 6	~1000	63.22	34.56	2771	0.55	-	M-Sr>?	2021	[74][*j]
287	$SrGd_{0.03}Fe_{11.97}O_{19}$	SG-AC	1100, 6	~1000	61.68	34.00	1241	0.55	-	M-Sr>?	2021	[74][*j]
288	$SrGd_{0.04}Fe_{11.6}O_{19}$	SG-AC	1100, 6	~1000	61.82	34.11	2692	0.55	-	M-Sr>?	2021	[74][*j]
289	$SrGd_{0.05}Fe_{11.5}O_{19}$	SG-AC	1100, 6	~1000	66.17	36.69	2954	0.55	-	M-Sr>?	2021	[74][*j]
290	$Sr_{0.975}Gd_{0.025}Fe_{12}O_{19}$	SG-PC	1100, 4	200-400	73.97	33.73	5090	0.45	1.00	M-Sr	2024	[73]
291	$Sr_{0.95}Gd_{0.05}Fe_{12}O_{19}$	SG-PC	1100, 4	200-400	69.86	31.67	5340	0.45	0.90	M-Sr	2024	[73]
292	$Sr_{0.925}Gd_{0.075}Fe_{12}O_{19}$	SG-PC	1100, 4	200-400	67.25	30.39	5450	0.45	0.83	M-Sr	2024	[73]
293	$Sr_{0.9}Gd_{0.1}Fe_{12}O_{19}$	SG-PC	1100, 4	200-400	67.46	30.85	3130	0.45	0.76	M-Sr	2024	[73]
	Strontium hexaferrite substituted with terbium											
294	$Sr_{0.9}Tb_{0.1}Fe_{12}O_{19}$	CP	850, 4	120	42.6	22.4	5126	0.52	-	M-Sr>Fe_2O_3	2016	[27]
295	$Sr_{0.9}Tb_{0.1}Fe_{12}O_{19}$	SG-AC	900, 2	~100	33.6	27.9	4355	0.54	0.89	M-Sr>Fe_2O_3	2019	[82]
296	$Sr_{0.9}Tb_{0.1}Fe_{12}O_{19}$	SG-AC	1100, 2	~500	30.7	27.9	5563	0.54	0.70	M-Sr>Fe_2O_3	2019	[82]
297	$Sr_{0.9}Tb_{0.1}Fe_{12}O_{19}$	SG-AC	1200, 2	~1000	62.6	29.3	6235	0.52	0.64	M-Sr>Fe_2O_3	2019	[82]
	Strontium hexaferrite substituted with dysprosium											
298	$Sr_{0.98}Dy_{0.02}Fe_{12}O_{19}$	HEM	1000, 15	1000-2000	58.70	25.80	1850	0.44	-	M-Sr	2023	[94][*k]
299	$Sr_{0.96}Dy_{0.04}Fe_{12}O_{19}$	HEM	1000, 15	1000-2000	61.60	27.50	2100	0.44	-	M-Sr	2023	[94][*k]
300	$Sr_{0.94}Dy_{0.06}Fe_{12}O_{19}$	HEM	1000, 15	2000	65.90	29.40	2425	0.44	-	M-Sr	2023	[94][*k]
301	$Sr_{0.92}Dy_{0.08}Fe_{12}O_{19}$	HEM	1000, 15	>2000	67.50	30.20	2500	0.45	-	M-Sr	2023	[94][*k]
302	$Sr_{0.9}Dy_{0.1}Fe_{12}O_{19}$	HEM	1000, 15	>2000	70.40	34.20	2690	0.48	-	M-Sr	2023	[94][*k]
303	$Sr_{0.85}Dy_{0.15}Fe_{12}O_{19}$	SG-MW	800, 1.3	41	58.70	26.13	2660	0.44		M-Sr>Fe_2O_3	2014	[45]
304	$Sr_{0.75}Dy_{0.25}Fe_{12}O_{19}$	SG-MW	800, 1.3	38	49.68	20.19	1411	0.40		M-Sr>Fe_2O_3	2014	[45]
305	$Sr_{0.5}Dy_{0.5}Fe_{12}O_{19}$	SG-MW	800, 1.3	32	28.84	15.21	6717	0.52		M-Sr~Fe_2O_3>$DyFeO_3$	2014	[45]
	Strontium hexaferrite substituted with holmium											
306	$Sr_{0.95}Ho_{0.05}Fe_{12}O_{19}$	SG-AC	1100, 4	320	73.24	36.36	5289	0.50	-	M-Sr	2024	[95]
307	$Sr_{0.9}Ho_{0.1}Fe_{12}O_{19}$	SG-AC	1100, 4	300	69.26	34.32	5362	0.50	-	M-Sr>Fe_2O_3	2024	[95]
308	$Sr_{0.85}Ho_{0.15}Fe_{12}O_{19}$	SG-AC	1100, 4	350	65.43	32.53	5460	0.50	-	M-Sr>Fe_2O_3	2024	[95]
309	$Sr_{0.8}Ho_{0.2}Fe_{12}O_{19}$	SG-AC	1100, 4	290	63.25	31.43	5443	0.50	-	M-Sr>Fe_2O_3, $HoFeO_3$	2024	[95]

(*continued on next page*)

Table 1 (*continued*)

ID	Chemical formula	Method	Sintering (°C, h)	Particle size (nm)	M_S (emu/g)	M_r (emu/g)	H_C(Oe)	(M_r/M_S)	BH_{max} (MGOe)	Phases	Year	Ref.
310	$SrHo_{0.05}Fe_{11.95}O_{19}$	SG-AC	1100, 4	342	76.73	38.35	5263	0.50	-	M-Sr	2024	[95]
311	$SrHo_{0.1}Fe_{11.9}O_{19}$	SG-AC	1100, 4	551	75.14	37.82	4885	0.50	-	M-Sr>Fe_2O_3	2024	[95]
312	$SrHo_{0.15}Fe_{11.85}O_{19}$	SG-AC	1100, 4	504	74.57	38.94	4754	0.50	-	M-Sr>Fe_2O_3	2024	[95]
313	$SrHo_{0.2}Fe_{11.8}O_{19}$	SG-AC	1100, 4	434	73.28	36.81	4786	0.50	-	M-Sr>$HoFeO_3$	2024	[95]
	Lead hexaferrite											
314	$PbFe_{12}O_{19}$	PPM	1000, 1	1500	54.20	30.80	2325	0.57	-	M-Pb	2015	[47]
315	$PbFe_{12}O_{19}$	SG-AC	900, 2	~2000	31.50	18.55	5123	0.58	-	M-Pb	2017	[96]
316	$PbFe_{12}O_{19}$	SG-AC	950, 0.75	17	61.38	45.06	1082	0.73	-	-	2018	[97]
317	$PbFe_{12}O_{19}$	SS	950, 2	~3000	52.00	23.00	950	0.44	-	M-Pb	2016	[98]
318	$PbFe_{12}O_{19}$	SG-AC	900, 2	500-1000	27.89	15.66	1880	0.56	-	M-Pb	2015	[99]
319	$PbFe_{12}O_{19}$	SG	800, 3	57	42.28	25.20	3872	0.59		M-Pb>Fe_2O_3	2016	[100]
320	$PbFe_{12}O_{19}$	SG-AC	950, 6	883	58.3	25.6	1429	0.44	-	M-Pb	2023	[101]
	Lead hexaferrite substituted with lanthanum											
321	$Pb_{0.9}La_{0.1}Fe_{12}O_{19}$	SS	1350, 2	>5000	63.3	17.7	400	0.28	-	M-Pb	2014	[102]
322	$Pb_{0.8}La_{0.2}Fe_{12}O_{19}$	SS	1350, 2	>5000	64.5	15.4	507	0.24	-	M-Pb	2014	[102]
323	$Pb_{0.7}La_{0.3}Fe_{12}O_{19}$	SS	1350, 2	>5000	66.7	3.3	120	0.05	-	M-Pb	2014	[102]
324	$Pb_{0.6}La_{0.4}Fe_{12}O_{19}$	SS	1350, 2	>5000	60.1	1.8	62	0.03	-	M-Pb	2014	[102]
325	$Pb_{0.5}La_{0.5}Fe_{12}O_{19}$	SS	1350, 2	>5000	53.4	4.2	133	0.08	-	M-Pb	2014	[102]
326	$Pb_{0.3}La_{0.7}Fe_{12}O_{19}$	SS	1350, 2	>5000	62.7	26.9	787	0.43	-	M-Pb	2014	[102]
	Calcium hexaferrite											
327	$CaFe_{12}O_{19}$	SG-AC	850, 2	~1600	29.97	17.20	3301	0.57	-	M-Ca	2024	[103]
328	$CaFe_{12}O_{19}$	SG	500, 3	4-16	37.67	2.28	18	0.06	-	M-Ca	2013	[104]
329	$CaFe_{12}O_{19}$	MM	950, 9	32-39	28.00	4.60	185	0.16	-	M-Ca	2024	[48]
330	$CaFe_{12}O_{19}$	SS	1200, 12	2260	0.56	0.19	736	0.31	-	M-Ca>Fe_2O_3	2023	[105]
	Calcium hexaferrite substituted with lanthanum											
331	$Ca_{0.5}La_{0.5}Fe_{12}O_{19}$	SG-AC	1100, 5	1710	22	13	1618	0.61	-	M-Ca	2024	[106]
332	$CaLa_{0.5}Fe_{11.5}O_{19}$	SG-AC	950, 4	168-259	0.59	0.11	1205	0.18	-	M-Ca	2019	[107]
333	$CaLa_1Fe_{11}O_{19}$	SG-AC	950, 4	168-259	0.55	0.09	404	0.17	-	M-Ca	2019	[107]
334	$CaLa_{1.5}Fe_{10.5}O_{19}$	SG-AC	950, 4	168-259	0.42	0.06	966	0.14	-	M-Ca	2019	[107]
335	$CaLa_2Fe_{10}O_{19}$	SG-AC	950, 4	168-259	0.36	0.05	1775	0.14	-	M-Ca	2019	[107]
	Calcium hexaferrite substituted with samarium											
336	$CaFe_{11.95}Sm_{0.05}O_{19}$	SG-AC	850, 2	~1600	33.45	19.47	2954	0.58	-	M-Ca	2024	[103]
337	$CaFe_{11.9}Sm_{0.1}O_{19}$	SG-AC	850, 2	~1600	39.93	23.01	2471	0.57	-	M-Ca	2024	[103]
338	$CaFe_{11.85}Sm_{0.15}O_{19}$	SG-AC	850, 2	~1600	43.54	24.79	2261	0.57	-	M-Ca	2024	[103]
339	$CaFe_{11.8}Sm_{0.2}O_{19}$	SG-AC	850, 2	~1600	44.03	25.27	2334	0.57	-	M-Ca	2024	[103]
	Calcium hexaferrite substituted with dysprosium											
340	$CaDy_{0.1}Fe_{11.9}O_{19}$	MM	950, 9	32-39	29.00	5.30	261	0.18	-	M-Ca	2024	[48]
341	$CaDy_{0.15}Fe_{11.85}O_{19}$	MM	950, 9	32-39	35.00	7.40	310	0.21	-	M-Ca	2024	[48]
342	$CaDy_{0.2}Fe_{11.8}O_{19}$	MM	950, 9	32-39	36.00	8.90	446	0.25	-	M-Ca	2024	[48]
343	$CaDy_{0.25}Fe_{11.75}O_{19}$	MM	950, 9	32-39	42.00	10.90	492	0.26	-	M-Ca	2024	[48]
344	$CaDy_{0.3}Fe_{11.7}O_{19}$	MM	950, 9	32-39	49.00	14.40	549	0.30	-	M-Ca	2024	[48]

[*a] Magnetization curves were measured using a maximum applied field of 3 kOe.
[*b] Magnetic properties were reported in the S.I. units.
[*c] Magnetizations M_r and M_S, reported in the table does not match with the magnetization curves.
[*d] Non determined phase is observed within the hexaferrite (probably ^{n}eodymium orthoferrite).
[*e] A non-determined minor phase is observed in the X-ray patterns.
[*f] Ba-hexaferrite was prepared with 1 and 2 %wt of Nd_2O_3 as additive.
[*g] $SmFeO_3$ seems to be present as secondary phase at ~33° in the X-ray patterns of samples with x = 0.5, 0.75 [108].
[*h] Presence of $GdFeO_3$ is observed in the X-ray patterns [109].
[*i] A non-determined minor phase is observed in the X-ray patterns.
[*j] A non-determined minor phase is observed in the X-ray patterns, probably Fe_2O_3.
[*k] The samples show high crystalline texture which can affect the magnetic properties.

of 45 mL ammonia and 15 mL polyethylene glycol into the precursor solution. The dispersion solution is maintained at 70 °C under stirring for 24 h and then moved out of the glove box. The water and organic molecules are removed from the dispersion solution by centrifugation at 12000 rpm. The remaining colloid powders were calcined at 450 °C for 1 h. The obtained powder is grinded and calcined at 800 °C for one hour to remove the organic components. Thus, pure hexaferrite powder in a single structure was obtained when it is subjected to a sintering procedure [48].

- **Microemulsion technique (MM).** The $Fe(NO_3)_3\ _9\ H_2O$ nitrate salts, and NaOH are used as chemicals in the synthesis of the hexaferrite. The metal nitrates are added to Pyrex glass beakers and dissolved in distilled water to prepare the required solutions. The solutions are stirred for 25 min at 60 °C and then, cetyltrimethylammonium bromide is added as surfactant. NH_4 OH (32 %) is added to maintain a pH = 11. The solution is continuously stirred for 7 h. After the stirring period, the contents are filtered and washed with deionized water until pH of 7. Then, the dried powder is annealed to synthesize the hexaferrite phase [49].

4. Rare earth substitutions

Increased interest in rare-earth substitution in the M-type hexaferrites has taken place over the past decade. At present, a large variety of rare earths have been used as substituent elements, studying the influence of rare earths on the structural, magnetic, dielectric, optical and absorption properties of the hexaferrite [50–52]. However, many of these properties also are affected by the fabrication method chosen for the hexaferrite obtainment. Currently, many variations to the fabrication methods have been proposed, involving different parameters to be considered and that affect the main properties of the hexaferrites. In particular, the fabrication method can affect particle growth, allowing to

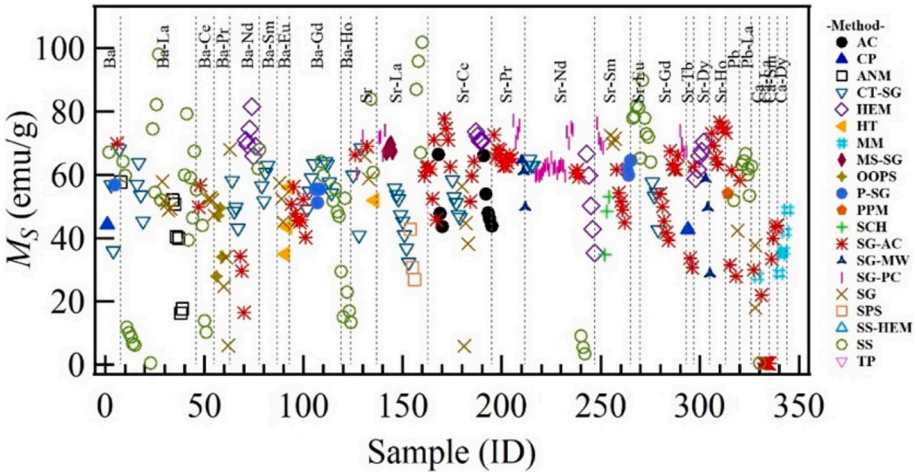

Fig. 2. Magnetization to saturation obtained for 344 samples of M-type hexaferrites substituted with rare earths prepared by various methods.

obtain hexaferrite particles from a few nanometers to various microns. Also, sintering temperature can influence the crystallization of the M-type hexaferrite, as well as the presence of secondary phases. All these factors hide the real influence of substitution of rare earths on the physical properties of the hexaferrite compounds. Thus, in this work we analyzed the magnetic properties of hexaferrites substituted with rare earths, considering the fabrication method, sintering conditions, and the presence of secondary phases. Our analysis only considers the single substitution of rare earths on the structure of the M-type hexaferrite, in both the divalent cation (Sr^{2+}, Ba^{2+}, Pb^{2+} and Ca^{2+}) and the trivalent iron cations (Fe^{3+}), reported in literature mainly during the last decade. Therefore, co- and multiple- substitutions involving rare earths were not taken into account.

Table 1 shows the compilation of analyzed samples involving rare earth substitutions within their magnetic properties and fabrication conditions. Additionally, the unsubstituted hexaferrites are included as reference points to evaluate the effects of the rare earth substitutions in the M-type hexaferrites. In the chemical formula indicates the type of rare earth used as the substituent, the amount of degree of substitution, and if rare earth substitutes the divalent or trivalent cation. In the first case, the general chemical formula is given by the Eq. (1), while the case that the rare earth substituted the iron cation is described by Eq. (2)

$$\left(Me^{2+}_{1-x}Re^{3+}_{x}\right)\left(Fe^{3+}_{12-x}Fe^{2+}_{x}\right)O_{19} \tag{1}$$

$$Me^{2+}\left(Fe^{3+}_{12-x}Re^{3+}_{x}\right)O_{19} \tag{2}$$

where Me is the divalent cation and Re is the trivalent rare earth used as the substituent element. In the table is indicated the fabrication method and sintering conditions. A brief description of each of these methods is provided in the previous section, although some variations or modifications may exist. It is therefore necessary to check the experimental details directly in the reference provided. The particle size is included because of its direct relationship with the behavior of the coercive field. Also, the secondary phases are reported based on the X-ray diffraction patterns for each sample and authors' own analysis. A simplified notation is used to point out the presence of second phases as well as the relative proportion regarding the M-type hexaferrite phase. For the analysis of the magnetic properties, there were reported four parameters obtained from the magnetization curves. The saturation magnetization (M_s), remanent magnetization (M_r), coercive field (H_c) and the squareness ratio (M_r/M_s). In addition, the maximum energy product $(BH)_{max}$ is reported in the cases in which this parameter was provided by the authors. However, this parameter is less frequency reported in the literature. In this table only have been considered the experimental works used the cgm units' system. For the magnetic properties presented in the SI units see the Table in supplementary information. This was done to facilitate comparisons purposes between different experimental works. The analysis is complete including the phases present in each one of the analyzed samples. For this, we consider the X-ray diffraction results alongside the magnetic properties.

5. Discussion and data analysis

A comprehensive analysis of the magnetic properties of the M-type hexaferrites has been conducted drawing upon a decade of reported data. While various factors, including sintering conditions and presence of secondary magnetic phases, can influence the magnetic properties of the M-type hexaferrites, our review of 344 samples highlights the significant impact of rare earth substitutions compared to unsubstituted M-type hexaferrites. This analysis shows behavior of the magnetic properties of the M-type hexaferrites. The data have been organized with the sample identifier (ID) indicated in Table 1. The fabrication method, type hexaferrite, and type of rare earth used as the substituent element are indicated with their respective magnetic properties. The samples based on the barium hexaferrite (M-Ba) correspond to the samples ID from 1 to 124, followed by the strontium based hexaferrites (M-Sr) have IDs from 125 to 313. The lead-based hexaferrites (M-Pb) have ID from 314 to 236, and from 327 to 344 for the calcium-based hexaferrites (M-Ca), the latter is the least studied probably because of the poor hard-magnetic properties.

The magnetization to saturation (M_S) obtained for the analyzed samples is shown in Fig. 2. In this graph, the average saturation value is close to 60 emu/g for most of the fabrication methods, while the highest M_S values have been reached using the solid-state method, spotlighting the substitution with lanthanum in the barium and strontium hexaferrites, and the strontium hexaferrite substituted with europium. While most samples regardless of their fabrication methods, achieve M_S values between 70–40 emu/g, the rare earth substitution, sintering route, and fabrication conditions play a crucial role in optimizing the hard-magnetic performance. On the other hand, samples prepared by the solid-state method show the highest and lowest M_S due to the tuneability of the microstructural characteristics and crystallinity attained by this method. Calcium hexaferrites consistently exhibit lower magnetization values regardless of the fabrication method or rare earth substitution. The lead-based hexaferrites show close M_S values than the ones of the strontium-based hexaferrites. Although not many rare earths have been reported as substituent elements of the lead hexaferrite. Fig. 2 offers an overview of the magnetization M_S behavior of rare earth substituted hexaferrites. However, achieving saturation magnetization is challenging due to the large magnetocrystalline anisotropy of hexaferrites [24,110,111]; which demands the application of very strong

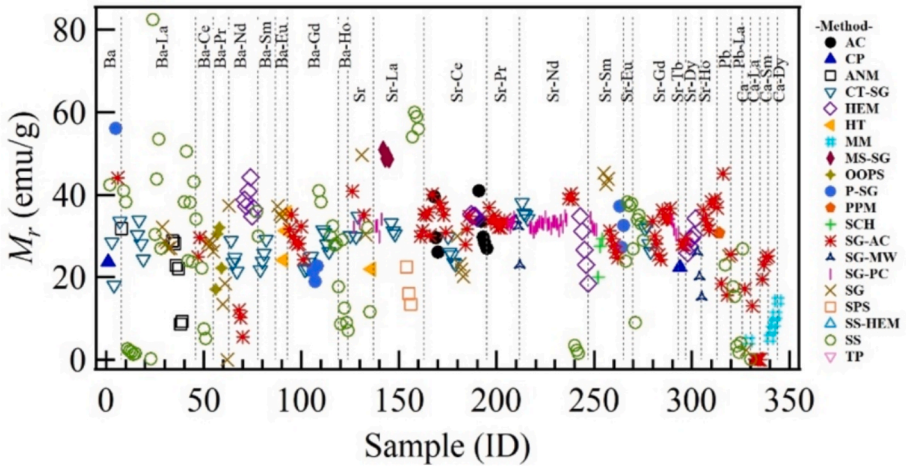

Fig. 3. Magnetization remanences reported for M-type hexaferrites substituted with rare earths.

magnetic fields.

Therefore, some authors report the magnetization reached at maximum applied field and other researchers use the law of approach to saturation for estimate the magnetization to saturation [112]. These methodological differences should be taken into account because they can induce small variations at the time of reporting the magnetization to saturation.

Several mechanisms have been proposed to explain the variation in saturation magnetization resulting from rare-earth substitution in M-type hexaferrites. In agreement with the charge compensation model, the formation of Fe^{2+} instead of Fe^{3+} in different crystallographic sites can change the magnetization to saturation because of the different magnetic moment of the Fe^{3+} ions (5.92 μ_B) regarding the Fe^{2+} ions (4.90 μ_B) [113]. A variation in saturation magnetization is also expected when a rare-earth cation replaces an iron cation, specified if the stoichiometry given by **Equation (2)** is satisfied. In these cases, it is critical for identifying the sites affected by substitution, because cations at sites 12 k, 2a, and 2b contain iron ions with up-spins (↑), which contributes to sum the net magnetic moment along the c-axis. Conversely, cations at sites $4f_1$ and $4f_2$ contain iron ions with down-spins (↓), reducing the net magnetic moment along the c-axis. Another way in which the magnetization to saturation can vary by effect of the rare earth substitution is thought to involve a change in the superexchange lengths. Superexchange lengths are critical parameters that strengthen magnetocrystalline anisotropy, thereby aligning the magnetic moments of iron cations parallel or antiparallel to the c-axis. Then, rare-earth substitution can induce changes in the crystal structure and superexchange lengths [23,24], potentially leading to canting movement of the magnetic moments and a subsequent variation in the net magnetic moment of the hexaferrite [114,115]. The substitution with rare earths can induce a variation in the magnetization to saturation of hexaferrites probably by a combination of various factors.

Fig. 3 shows the behavior of the magnetization to remanence (M_r). The results suggest that the highest magnetizations to remanence are achieved using lanthanum. Although, the lanthanum substitution in hexaferrites has been more extensively studied than other rare earth elements resulting in a larger existence of available data. The average saturation magnetization of the majority of the samples is below than 45 emu/g. The observed behavior of the magnetization to remanence could be attributed to a combination of factors. Interparticle interactions, the emergence of both magnetizing and demagnetizing-like interactions, the presence of impurities and secondary phases, and the crystalline texture can all significantly impact the magnetization to saturation of substituted hexaferrites [116,117]. Then, although the rare earth substitutions can influence the magnetization to saturation, it does not appear to have a substantial impact on the magnetization to remanence.

Fig. 4 shows the magnetic squareness ratio (SQR = M_r/M_S), a characteristic parameter that depends on the anisotropy of the system, and which allow us to evaluate the magnetic hardness of the hexaferrites [118,119]. SQR varies from 0 to 1, usually a squareness ratio $M_r/M_S \approx 0.5$ indicated that particles have uniaxial anisotropy and they are randomly distributed. In the case that $M_r/M_S \ll 0.5$ the particles have a

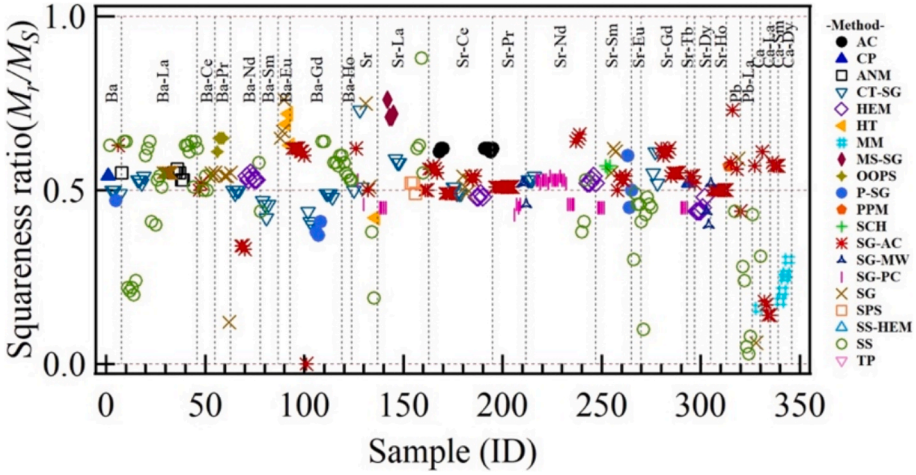

Fig. 4. Remanence squareness calculated from data of M-type hexaferrites substituted with rare earths.

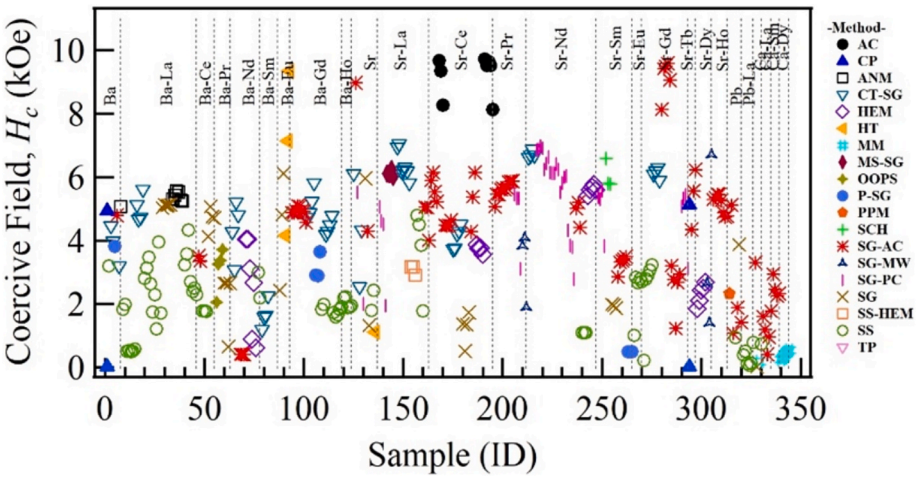

Fig. 5. Coercive field of rare earth substituted hexaferrites fabricated through various synthesis routes during the last decade.

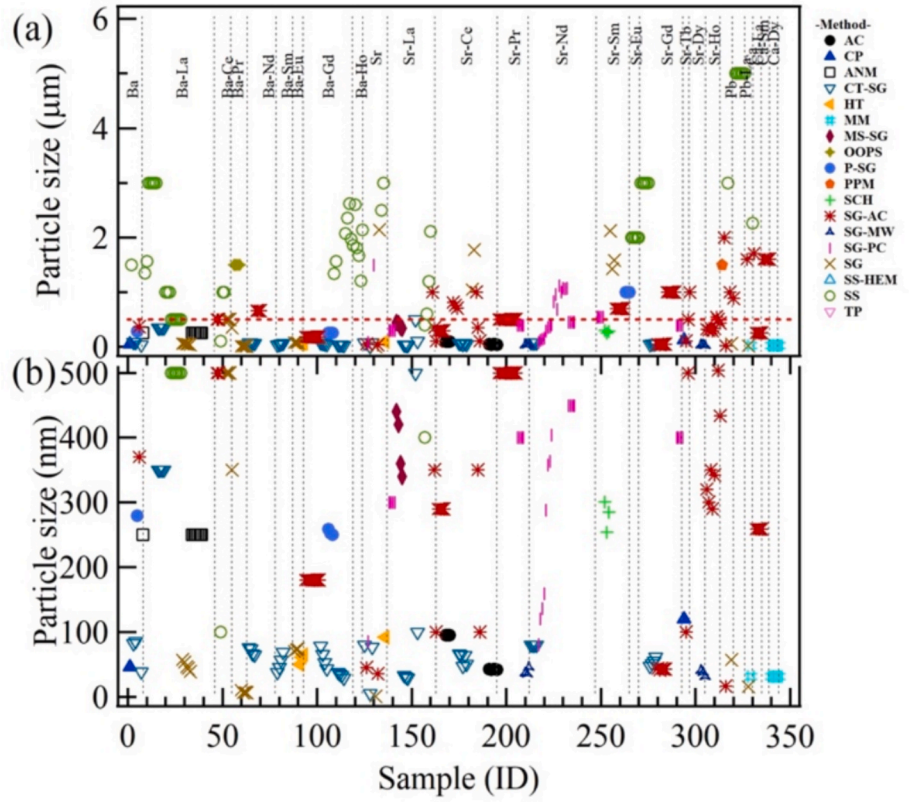

Fig. 6. (a) Particle size obtained for hexaferrites prepared by different fabrication methods. (b) View showing the samples that have particle sizes below than 500 nm.

magnetic multi-domain structure. Also, if the squareness ratio $M_r/M_S >$ 0.5, the hexaferrite particles are in a single-domain magnetic structure. M_r/M_S values larger than 0.7 can be usually obtained with hexaferrite nanoparticles, and above 0.8 when interparticle interaction is controlled [120]. In this sense, the emergence of magnetostatic inter-particles interactions gives a reduction of SQR [118,119]. Then, the magnetic squareness ratio can provide a measure of the magnetic-domains structure, the uniaxial anisotropy and can help to identify changes on the interaction state of the hexaferrite particles [121–123].

Fig. 4 shows that the hexaferrites, regardless of their methods of obtaining and type of substitutions, have SQR value around of 0.5. This figure also reveals that it is possible to obtain substituted hexaferrites with very high SQR value; for example in the case of the sample ID 90 and 92 (substituted with Eu); 128 and 131 (Sr-unsubstituted); 143, 144, 145, and 159 (substituted with La); and 316 (Pb-unsubstituted), all of these with SQR > 0.7. The obtention of high SQR values is favorable in the field of hard magnetic applications. However, high SQR values only can be reached by controlling the rare earth substitution and the magnetic domains structure. The substitution with lanthanum and europium showed to be higher SQR values. Moreover, lead hexaferrite have significant SQR value, which is almost comparable to the ones exhibited by the strontium hexaferrite.

Fig. 5 shows the behavior of the coercive field showed by the analyzed samples. The fabrication method and type of rare earth used as

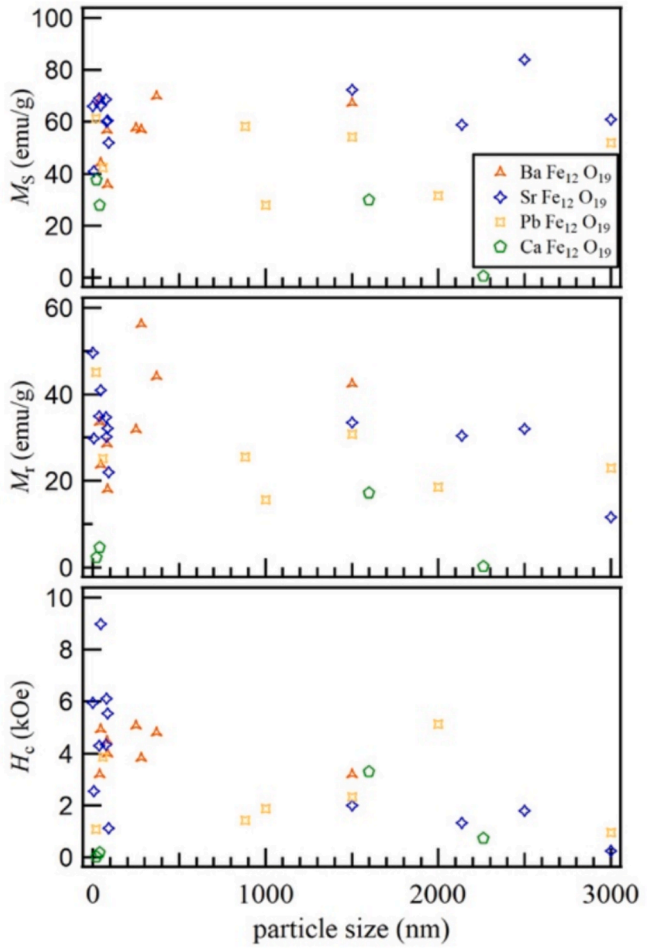

Fig. 7. Effect of particle size on the magnetic properties: magnetization to saturation, magnetization to remanence and coercive field for the unsubstituted (pure) M-type hexaferrites.

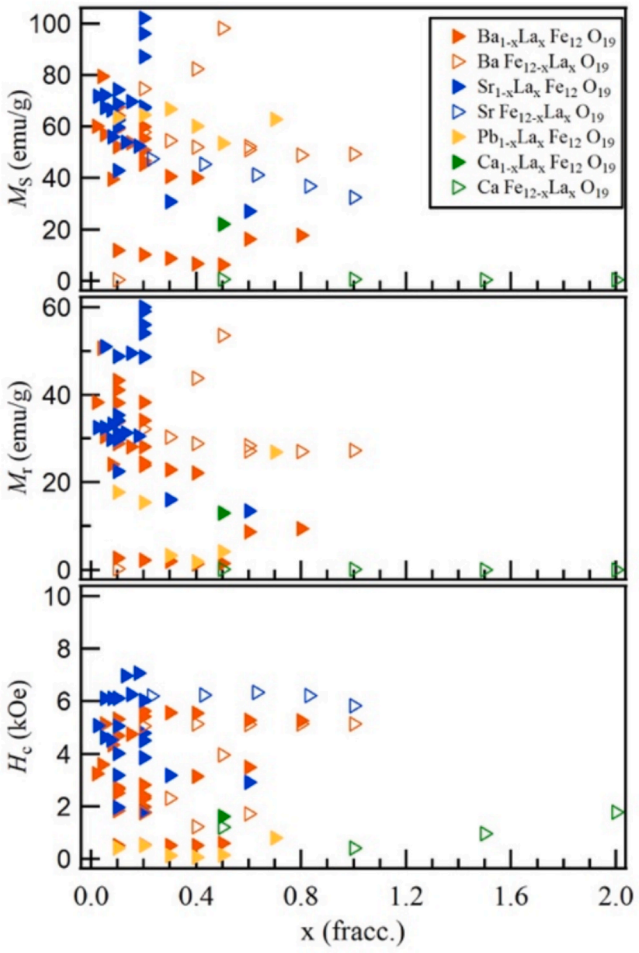

Fig. 8. Magnetic properties, M_S, M_r and H_c plotted as a function of lanthanum substitution fraction (x), for the (Ba, Sr, Pb and Ca) M-type hexaferrites. (Filled symbols shows the substitution of the divalent cation while the open symbols show the substitution of the iron cations.

substituent element are indicated for a guide. The higher coercive field reached for the rare earth substituted hexaferrites is close to 10 kOe obtained for the hexaferrites with Eu, Ce, and Gd, and fabricated by chemical methods such as hydrothermal, sol–gel, and auto combustion. The average coercive field showed by the majority of the rare earth substituted hexaferrites are from 2 to 6 kOe. For permanent magnets, the coercive field is first related to the magnetocrystalline anisotropy and secondly the particle size distribution [124,125]. Rare earth substitution significantly alters the magnetocrystalline anisotropy. This may occur because rare earth cations could occupy some iron sites within the crystal structure. The presence of these rare earth ions can modify the electrostatic interactions with the surrounding ligands and to change the electrostatic forces, that subsequently influences the distribution of electron charges within the local environment of the iron sites. A maximum value of coercive field would be understood as the optimal particle size according to the stable single domain region [126]. In the single domain region, the coercive field is a function of the crystallite size. Also, coercive field follow a tend to decrease with reduction of particle size in the single domain region because of thermal effects [127].

Fig. 6**(a)** shows the particle size reported for hexaferrites fabricated by various methods. Hexaferrites with the largest particle sizes after sintering are typically produced using the solid-state method. This is result of the bigger particle size of the chemical precursors, oxides and carbonates, usually used in this method, and the higher sintering temperatures required to crystallize the M-type structure. Chemical methods allow a better control of the particle growth, allowing the obtention of hexaferrites with particle size below than 1 μm. In this case, temperature and sintering time significantly influence particle growth primarily through the process of particle coalescence. Chemical methods also allow the obtention of nanoparticles, see Fig. 6**(b)**. In this case, rare earth-substituted nano-hexaferrites have been synthesized using various chemical methods, including autocombustion, sol–gel, hydrothermal, and coprecipitation. While rare earth ions can sometimes act as particle growth inhibitors, the primary influence on particle size is typically attributed to sintering conditions.

Fig. 7 shows the magnetic properties of the unsubstituted Ba, Sr, Pb and Ca hexaferrites as a function of the particle size. It can be observed that barium and strontium hexaferrites reaches the maximum magnetization to saturation and remanence, closely followed by the lead hexaferrite. The magnetizations M_r and M_S, doesn't follow a clear tendency regarding the increase of the particle size. However, the increase of the particle size clearly tends to reduce the coercive field of hexaferrites. Therefore, the magnetic properties of the Ba, Sr and Pb hexaferrites show an improvement when the particle size is below than 500 nm. In compassion, the calcium hexaferrite always maintain a low magnetic performance.

Figs. 8 to 15 illustrates the magnetic properties of the rare earth substituted hexaferrites, drawing data from Table 1**.** The magnetic parameters M_S, M_r and H_c have been plotted as a function of the fraction of rare earth used as substituent (x). The plots in the figure are categorized by the specific rare earth element used as the substituent: lanthanum

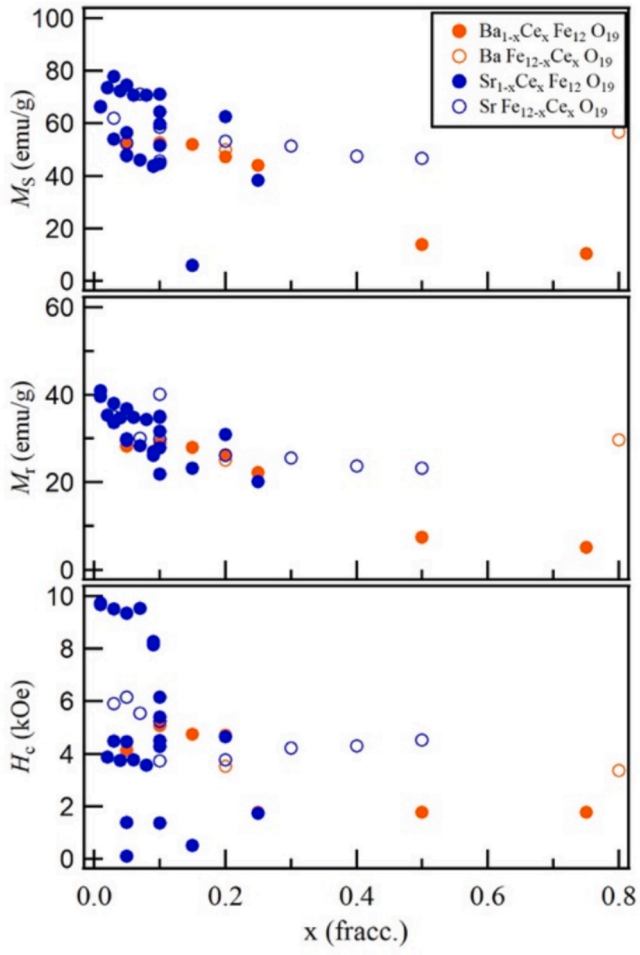

Fig. 9. Magnetic properties, M_S, M_r and H_c plotted as a function of cerium substitution fraction (x), for the (Ba and Sr) M-type hexaferrites.

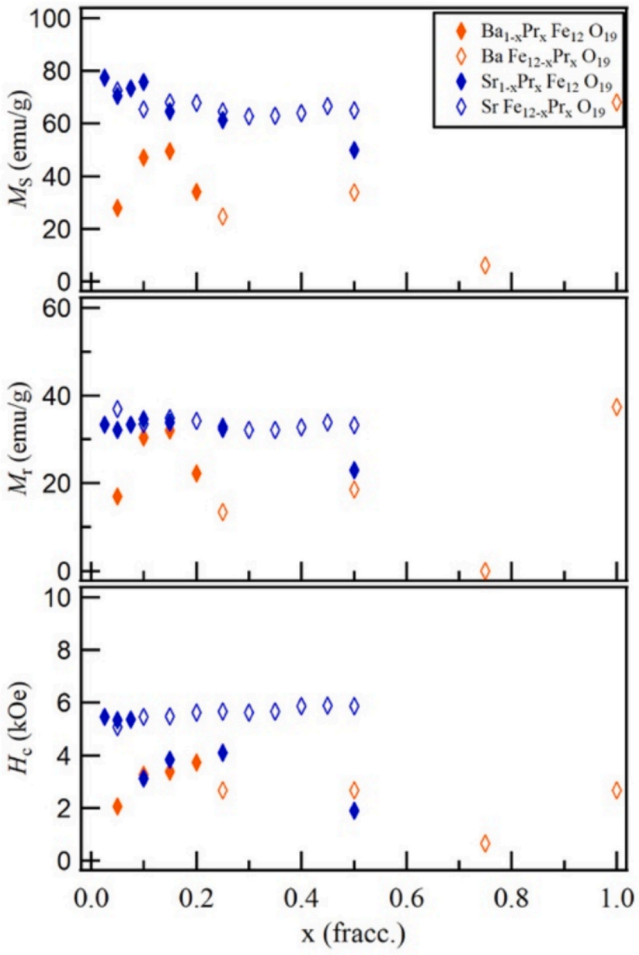

Fig. 10. Magnetic properties, M_S, M_r and H_c plotted as a function of praseodymium substitution fraction (x), for the (Ba and Sr) M-type hexaferrites.

(Fig. 8), cerium (Fig. 9), praseodymium (Fig. 10), neodymium (Fig. 11), samarium (Fig. 12), europium (Fig. 13), gadolinium (Fig. 14), holmium, dysprosium and terbium (Fig. 15). Filled symbols represent samples where the rare earth substituted the divalent cations (Ba^{2+}, Sr^{2+}, Pb^{2+}, and Ca^{2+}), while open symbols indicate the rare earths substituted the iron cations (Fe^{3+}). In both cases, the chemical stoichiometry is given for Equations (1) and (2). These plots are useful to summarize the behavior of the magnetic properties of the rare earth substituted hexaferrites, indicating the maximum and minimum values according to the fraction of substituent. It's important to acknowledge that the properties of hexaferrites could differ significantly depending on whether the rare earth substitutes divalent cations (filled symbols) or iron cations (open symbols). Despite this, useful correlations can be established between the type of rare earth element and the substitution fraction (x) by analyzing the magnetic properties of the substituted hexaferrites presented in these plots. For instance, a common trend observed is an initial enhancement of the magnetization in the hexaferrites at low rare earth substitution levels, typically in the range $0 < x < 0.1$ (the behavior of the magnetic properties for samples at $x = 0$ was presented in Fig. 7). However, a reduction of the magnetic properties is frequently observed at high rare earths contents. Although it's important to note that this is not a general rule, as can be seen by the samples substituted with praseodymium, where the magnetization properties remain relatively constant.

The observed enhancement of magnetic properties at low rare earth substitution levels can be attributed to an increase in the magnetocrystalline anisotropy, as a result of the rare earths incorporation in the crystalline structure of M-type hexaferrites. This behavior is interesting despite the various factors which can significantly influence the magnetic properties. The reviewed data suggest that low-level rare earth substitution may be an effective strategy for improving the magnetic properties of hexaferrites.

The effect of the rare earth substitution in the maximum energy product $(BH)_{max}$ is shown in Fig. 16. Unsubstituted strontium hexaferrite is presented as a reference and the different rare earths are correctly indicated. The highest $(BH)_{max}$ has been reached using praseodymium as substituent element, followed by samples with neodymium, samarium, and gadolinium. Also, better results can be obtained from the strontium hexaferrite instead of the barium or lead hexaferrites. While these results suggest that rare earth substitution can enhance the magnetic performance of hexaferrites, several factors significantly influence this outcome, including fabrication methods, sintering conditions, and the solubility limit of rare earth elements. Nevertheless, it is evident that a thoughtful rare earth substitution can lead to a substantial improvement in the maximum energy product.

6. Relevant aspects of the rare earth substitution in M-type hexaferrites

The use of rare earths as substituent elements in the structure of M-type hexaferrites has been of great interest in the past decade. Significant knowledge has been obtained by different research groups contributing to understand the effects of the rare earth substitution in the physical properties, namely the structural, magnetic and electrical

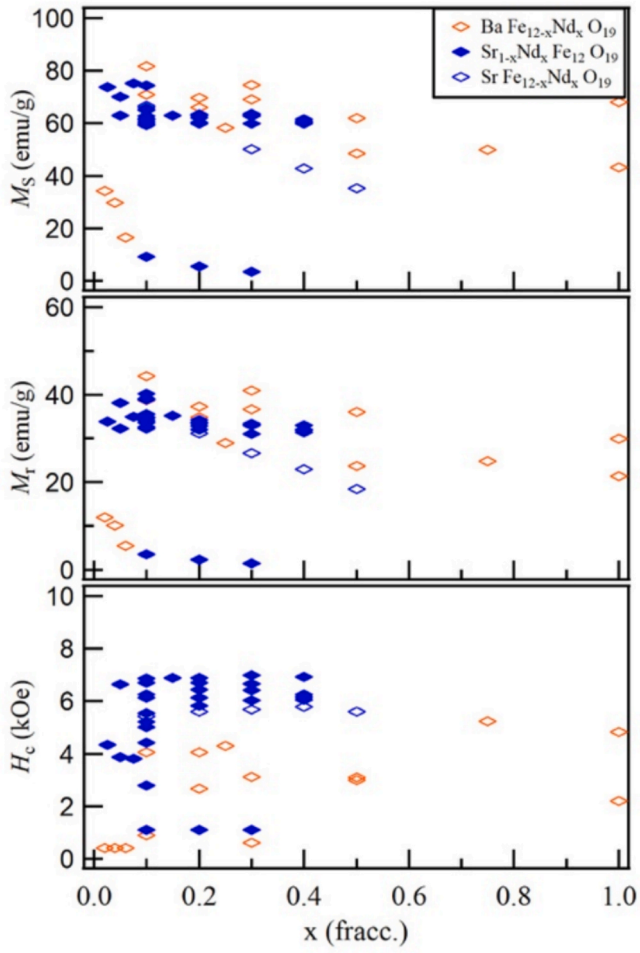

Fig. 11. Magnetic properties, M_S, M_r and H_c plotted as a function of neodymium substitution fraction (x), for the (Ba and Sr) M-type hexaferrites.

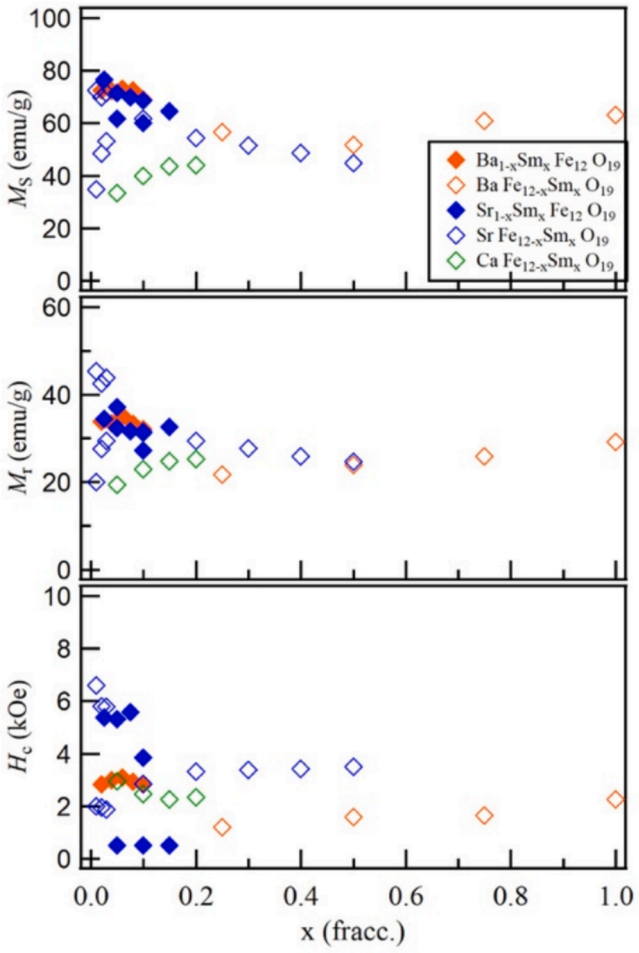

Fig. 12. Magnetic properties, M_S, M_r and H_c plotted as a function of samarium substitution fraction (x), for the (Ba, Sr, and Ca) M-M-type hexaferrites.

ones. Rare earths have the potential of modifying the intrinsic properties of hexaferrites. However, several aspects inhibit the application of rare earths in hexaferrites for permanent magnets. Below we will indicate some of the most relevant aspects of the use of rare earths as substituent elements in M-type hexaferrites.

- Rare earths definitely improve the magnetic performance of hexaferrites, and better results are generally obtained at very low rare earth contents (x), which can minimize the economic impact of developing rare-earths substituted hexaferrites.
- Rare earth elements are currently expensive and scarce, and the improvement in maximum energy product achieved so far does not justify. the use of hexaferrites with rare earths for industrial or commercial applications in field of permanent magnets.
- New strategies have recently been adopted to achieve significant improvement of the magnetic properties of hexaferrites, one of the most studied deals about the multiple substitutions, involving rare earths and other cations to promote a synergic effect that may allow to enhance the magnetic yield of the M-type hexaferrites.
- Although the impact of substitution of rare earths on the magnetic properties of the hexaferrites can be moderate, definitely rare earths affects the electronic and structural properties, that can be of interest in developing of novel technologies. Besides, the effects of rare earth substitution on magneto-optical and magneto-electric couplings make of the rare earth substitution an interesting research field for the next years with high potential for electronic applications.

7. Future perspectives

Research on rare earth-substituted M-type hexaferrites has substantially advanced our understanding of how these elements modify crystal structure, microstructural attributes, and magnetic performance. Nonetheless, several open challenges persist, and addressing them will be essential to fully harness the capabilities of these promising ferrimagnetic oxides.

A central issue involves maintaining a high phase purity. Although high-temperature sintering can promote crystallinity, it may inadvertently favour the formation of secondary phases (e.g., orthoferrites). Meanwhile, low-temperature chemical methods such as sol–gel or hydrothermal synthesis may yield nanosized particles with minimal impurities but sometimes compromise crystallinity [128]. Future efforts could systematically correlate synthesis parameters—choice of precursors, complexing agents, and heating profiles—with the relative phase composition and degree of rare earth incorporation, thereby enabling rational design rules for scalable and repeatable fabrication. Furthermore, advanced processing approaches such as spark plasma sintering, molten salt synthesis, or microwave-assisted calcination show promise in optimizing densification and grain growth at reduced thermal budgets, ensuring both improved magnetic properties and a more sustainable production process [129].

From a fundamental standpoint, the detailed site occupancy of rare earth ions in the five distinct interstitial sublattices remains insufficiently understood. Novel studies would reveal not only how these cations distribute within the hexaferrite lattice but also how their

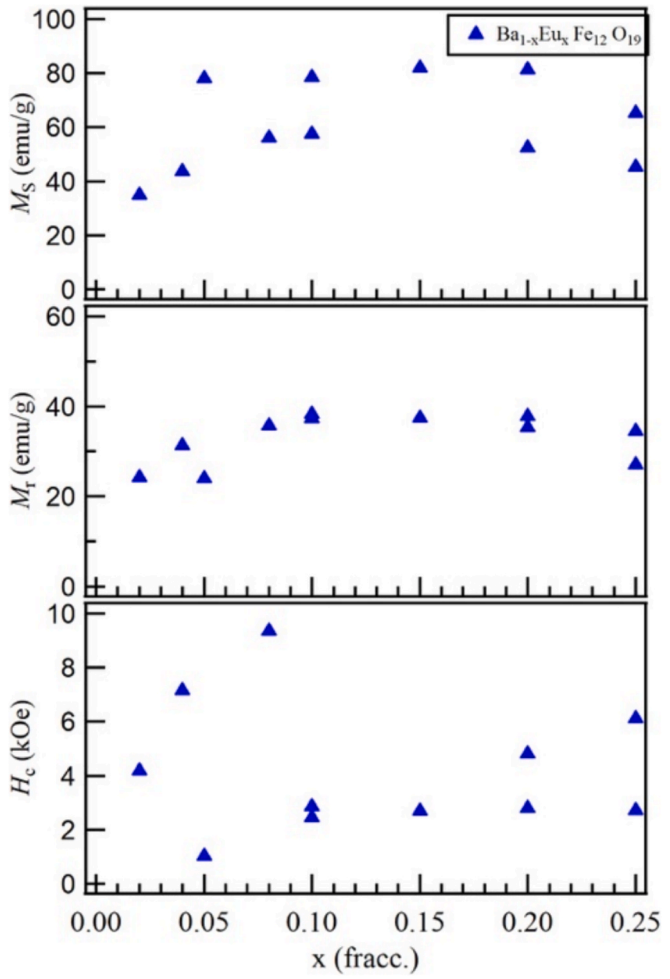

Fig. 13. Magnetic properties, M_S, M_r and H_c plotted as a function of europium substitution fraction (x), for the barium M-type hexaferrites.

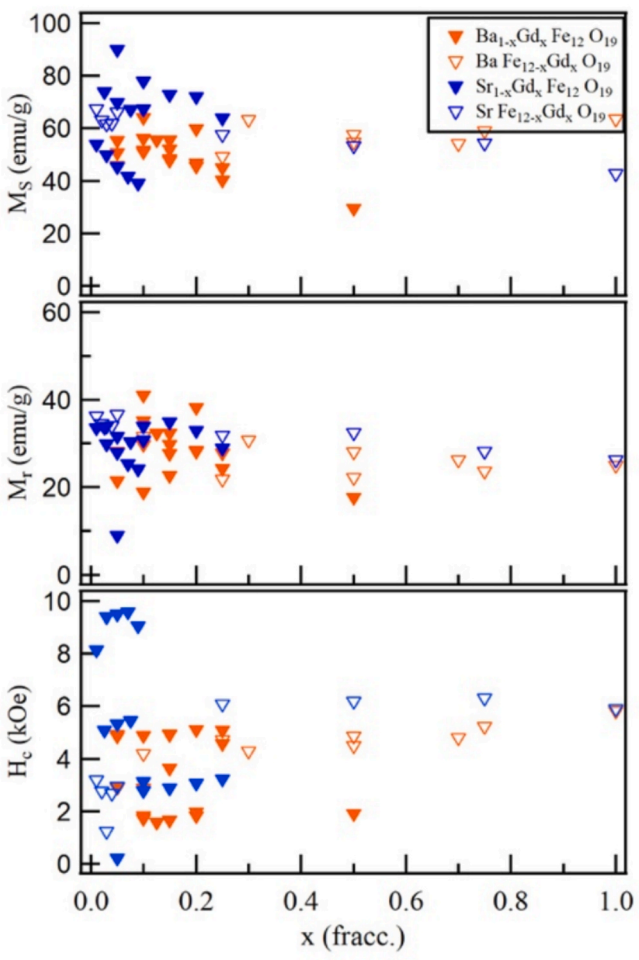

Fig. 14. Magnetic properties, M_S, M_r and H_c plotted as a function of gadolinium substitution fraction (x), for the (Ba and Sr) M-type hexaferrites.

placement influences superexchange interactions and magnetocrystalline anisotropy. This knowledge could then guide Co-substitution strategies (e.g., combining rare earth and transition metal) to tailor coercivity, remanence, and the squareness ratio in a more predictable manner [130]. Concurrently, real-time in situ probes of the heat treatment stage could uncover transient intermediate phases or subtle reaction pathways, allowing dynamic intervention to promote the pure M-type phase.

Beyond structural optimization, it is worth exploring hybrid or composite systems in which rare earth-substituted hexaferrites are coupled with other magnetic or functional phases to achieve new or enhanced properties. Potential applications range from permanent magnets and microwave devices to electromagnetic interference (EMI) shielding, energy storage, and spintronic devices. In particular, substituting scarce or costly rare earths (e.g., Nd, Dy) with more abundant or recycled ones represents a promising strategy toward sustainable permanent magnet technologies. Ultimately, combining systematic experimental research with theoretical modelling—such as density functional theory (DFT) and micromagnetic simulations—will accelerate the design of hexaferrite-based components that meet the growing demand for multifunctional magnetic materials.

Overall, the coming years offer an array of opportunities to refine synthesis protocols, deepen our grasp of substitution mechanisms, and broaden the range of applications for rare earth-substituted M-type hexaferrites. Addressing these directions will be key to unlocking the full potential of these compounds in next-generation magnetic technologies.

8. Conclusion

This review paper exhaustively examined recent progress in incorporating rare earth elements into M-type hexaferrites, specifically analyzing their impact on magnetic properties. The effect of the rare earth substitution in M-type hexaferrites were discussed considering the influence of the fabrication method and the sintering conditions. A comprehensive table was compiled to summarize the results of experimental research conducted over the past decade. This table is a useful tool facilitates easy access to the relevant data, including fabrication conditions and the magnetic properties. Furthermore, the data analysis provides valuable insights into the current state of knowledge and the progress made in this field. Therefore, we emphasize the versatility and significant properties of M-type hexaferrites as a class of highly advantageous multifunctional materials, that plays a pivotal role in the advancement of modern technology.

CRediT authorship contribution statement

A. Lobo-Guerrero: Writing – review & editing, Supervision, Investigation, Conceptualization. **V.E. Salazar-Muñoz:** Writing – original draft, Supervision, Formal analysis. **R.H. Aguilera Del Toro:** Validation, Investigation, Formal analysis. **E.E. Hernández-Vázquez:** Resources, Methodology, Investigation.

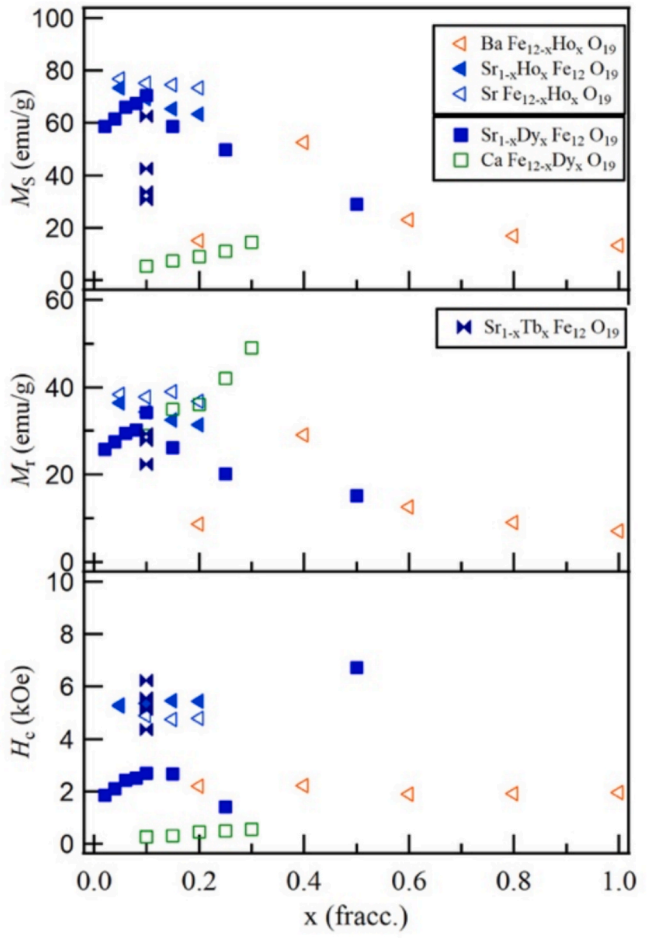

Fig. 15. Magnetic properties, M_S, M_r and H_c plotted as a function of holmium, dysprosium and terbium substitution fraction (x), for the (Ba and Sr) M-type hexaferrites.

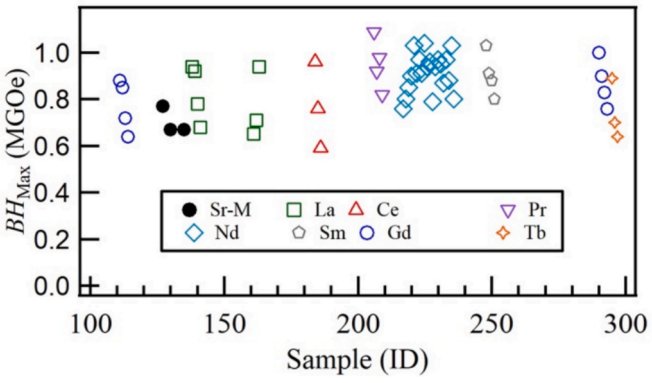

Fig. 16. Maximum energy product $(BH)_{max}$ reported for the M-type hexaferrites substituted with rare earths. (The strontium hexaferrite is shown as comparison).

Declaration of competing interest

The authors declare that they have no known competing financial interests or personal relationships that could have appeared to influence the work reported in this paper.

Acknowledgement

E.E.H.V. thanks SECIHTI (México) for her postdoctoral fellowship.

Appendix A. Supplementary data

Supplementary data to this article can be found online at https://doi.org/10.1016/j.jmmm.2025.173132.

Data availability

Data will be made available on request.

References

[1] V. Pratap Singh, R. Jasrotia, R. Kumar, P. Raizada, S. Thakur, K.M. Batoo, M. Singh, A current review on the synthesis and magnetic properties of M-type hexaferrites material, World J. Condensed Matter. Phys. 8 (2018) 36–61, https://doi.org/10.4236/wjcmp.2018.82004.

[2] P. Dhiman, G. Rana, D. Goyal, A. Goyal, Basics of ferrites: types and structures, in: G.K. Bhargava, S. Bhardwaj, M. Singh, K.M. Batoo (Eds.), Ferrites and Multiferroics, Engineering Materials, Springer, Singapore, 2021, https://doi.org/10.1007/978-981-16-7454-9_1R.

[3] R. Collongues, D. Gourier, A. Kahn-Harari, A.M. Lejus, J. Thery, D. Vivien, Magnetoplumbite-related oxides, Ann. Rev. 20 (1990) 51–82, https://doi.org/10.1146/annurev.ms.20.080190.000411.

[4] C. Pullar, Hexagonal ferrites: a review of the synthesis, properties and applications of hexaferrite ceramics, Prog. Mater Sci. 57 (2012) 1191–1334, https://doi.org/10.1016/j.pmatsci.2012.04.001.

[5] L.H. Lewis, F. Jiménez-Villacorta, Perspectives on permanent magnetic materials for energy conversion and power generation, Metall. Mater. Trans. A 44 (2012) 2–20, https://doi.org/10.1007/s11661-012-1278-2.

[6] H. Kojima, Fundamental properties of hexagonal ferrites with magnetoplumbite structure. Handbook of ferromagnetic materials, vol. 3. (1982), Elsevier, pp 305–391.

[7] S.A. Mathews, D. Rajan Babu, Analysis of the role of M-type hexaferrite-based materials in electromagnetic interference shielding, Curr. Appl Phys. 29 (2021) 39–53, https://doi.org/10.1016/j.cap.2021.06.001.

[8] L. Klemenz, A. Richter, N. Langhof, M. Göbbels, Structure and principles of oxidic hexaphases: a review, Open Ceram. 7 (2021) 100142, https://doi.org/10.1016/j.oceram.2021.100142.

[9] R. Valenzuela, Magnetic Ceramics, Cambridge University Press, Cambridge, 2005.

[10] A.S. Mikheykin, E.S. Zhukova, V.I. Torgashev, A.G. Razumnaya, Y.I. Yuzyuk, B. P. Gorshunov, A.S. Prokhorov, A.E. Sashin, A.A. Bush, M. Dressel, Lattice anharmonicity and polar soft mode in ferrimagnetic M-type hexaferrite $BaFe_{12}O_{19}$ single crystal, Eur. Phys. J. B 87 (2014) 232, https://doi.org/10.1140/epjb/e2014-50329-4.

[11] R.N. Summergrad, E. Banks, New hexagonal ferrimagnetic oxides, J. Phys. Chem. Solid 2 (1957) 312–317, https://doi.org/10.1016/0022-3697(57)90076-8.

[12] A. Deschamps, F. Bertaut. Substitution of a rare earth for barium in BaO. $6Fe_2$, O_3. Compt. Rend. 244 (1957) 3069–72.

[13] V.L. Moruzzi, M.W. Shafer, Phase equilibria in the system La_2O_3—iron oxide in air, J. Am. Cer. Soc. 43 (1960) 367–372, https://doi.org/10.1111/j.1151-2916.1960.tb13673.x.

[14] A. Aharoni, M. Schieber, Magnetic moment of lanthanum magnetoplumbite ferrite, Phys. Rev. 123 (1961) 807–809, https://doi.org/10.1103/PhysRev.123.807.

[15] I.N. Frantsevich, L.N. Tul'chinskii, Lanthanum-substituted barium hexaferrites, Powder Metall. Met. Ceram. 10 (1971) 133–137, https://doi.org/10.1007/BF00796412.

[16] F.K. Lotgering, A.M. Van Diepen, Electron exchange between Fe2+ and Fe3+ ions on octahedral sites in spinels studied by means of paramagnetic Mössbauer spectra and susceptibility measurements, J. Phys. Chem. Solid 38 (1977) 565–572, https://doi.org/10.1016/0022-3697(77)90221-9.

[17] F.K. Lotgering, Magnetic anisotropy and saturation of $LaFe_{12}O_{19}$ and some related compounds, J. Phys. Chem. Solid 35 (1974) 1633–1639, https://doi.org/10.1016/S0022-3697(74)80176-9.

[18] P.P. Kirichok, N.B. Voronina, O.F. Verezhak, V.Y. Garmash, Effect of additions of praseodymium and bismuth oxides on the properties of barium hexaferrites, Powder Metall. Met. Ceram. 24 (1985) 229–232, https://doi.org/10.1007/BF00795836.

[19] P.P. Kirpichok, N.B. Voronina, A.F. Sitnikov, V.Y. Garmash, Effect of rare-earth oxides on the magnetic properties of anisotropic barium ferrites, Soviet Phys. J. 32 (1989) 26–30, https://doi.org/10.1007/BF00896728.

[20] A. Bollero, E.M. Palmero, Recent advances in hard -ferrite magnets, Modern Permanent Magnets Woodhead Publishing Series in Electronic and Optical Materials (2022) 65–112, https://doi.org/10.1016/B978-0-323-88658-1.00013-3.

[21] N. Kostevšek, I. Serša, Characterization of metal-based nanoparticles as contrast agents for magnetic resonance imaging, Compreh. Anal. Chem., Chapter 9 (93) (2021) 303–343, https://doi.org/10.1016/bs.coac.2021.01.007.

[22] V. Chlan, K. Kouril, K. Ulicná, H. Stepánková, Charge localization and magnetocrystalline anisotropy in La, Pr, and Nd substituted Sr hexaferrites, Phys. Rev. B 92 (2015) 125125, https://doi.org/10.1103/PhysRevB.92.125125.

[23] M. Küpferling, R. Grössinger, M.W. Pieper, G. Wiesinger, H. Michor, Structural phase transition and magnetic anisotropy of La-substituted M-type Sr hexaferrite M-type Sr hexaferrite, Phys. Rev. B 73 (2006) 144408, https://doi.org/10.1103/PhysRevB.73.144408.

[24] W. Weber, C.H. Back, A. Bischof, D. Pescia, R. Allenspach, Magnetic switching in cobalt films by adsorption of copper, Nature 374 (1995) 788–790, https://doi.org/10.1038/374788a0.

[25] C. Bhandari, M.E. Flatté, D. Paudyal, Enhanced magnetic anisotropy in lanthanum M-type hexaferrites by quantum-confined charge transfer, Phys. Rev. Mater. 5 (2021) 094415, https://doi.org/10.1103/PhysRevMaterials.5.094415.

[26] M. Jamalian, A. Ghasemi, M.J. Pourhosseini Asl, Magnetic and microwave properties of barium hexaferrite ceramics doped with Gd and Nd, J. Electron. Mater. 44 (2015) 2856–2861, https://doi.org/10.1007/s11664-015-3720-x.

[27] S. Malhotra, M. Chitkara, I. Singh Sandhu, N. Dawar, J. Singh, Investigation of structural, magnetic and dielectric properties of terbium doped strontium hexaferrite for high frequency applications, Ind. J. Sci. Technol. 9 (2016) 1–10, https://doi.org/10.17485/ijst/2016/v9i27/96638.

[28] D. Shekhawat, S. Verma, P. Sharma, Effect of La on magnetic properties of $BaFe_{12}O_{19}$, Trans. Indian Cer. Soc. 76 (2017) 247–251, https://doi.org/10.1080/0371750X.2017.1396925.

[29] Y. Taryana, A. Manaf, W. Ari Adi, Change of structure and magnetic properties of La substituted barium hexaferrite, IOP Conf. Series J. Phys.: Conf. Series 1282 (2019) 012045, https://doi.org/10.1088/1742-6596/1282/1/012045.

[30] H. Kumar Satyapal, R. Kumar Singh, N. Kumar, S. Sharma, Low temperature synthesis and influence of rare earth Nd^{3+} substitution on the structural, magnetic behaviour of M-type barium hexaferrite nanomaterials, Mater. Today Proc. 28 (2020) 234–240, https://doi.org/10.1016/j.matpr.2020.01.590.

[31] S. Sharma, H. Kumar Satyapal, S. Sonu Kumar, R. Aryan, A. Manash, V. Kumar, Effect of Gd^{3+} substitution on the structural and magnetic properties of barium hexaferrite nanomaterials, Mater. Today Proc. 44 (2021) 2587–2592, https://doi.org/10.1016/j.matpr.2020.12.650.

[32] M.A.P. Buzinaro, B.F.O. Costa, M.S. Ivanov, G.C. Cunha, M.A. Macêdo, R. S. Angélica, N.S. Ferreira, Investigations on the structural and magnetic properties of $Ba_{1-x}Gd_xFe_{12}O_{19}$ ($0 \leq x \leq 0.15$) nanoparticles, J. Magn. Magn. Mater. 555 (2022) 169340, https://doi.org/10.1016/j.jmmm.2022.169340.

[33] M.A.P. Buzinaro, N.S. Ferreira, F. Cunha, M.A. Macêdo, Hopkinson effect, structural and magnetic properties of M-type Sm^{3+}-doped $SrFe_{12}O_{19}$ nanoparticles produced by a proteic sol-gel process, Cer. Inter. 42 (2016) 5865–5872, https://doi.org/10.1016/j.ceramint.2015.12.130.

[34] H. Sözeri, İ. Küçük, H. Özkan, Improvement in magnetic properties of La substituted $BaFe_{12}O_{19}$ particles prepared with an unusually low Fe/Ba molar ratio, J. Magn. Magn. Mater. 323 (2011) 1799–1804, https://doi.org/10.1016/j.jmmm.2011.02.012.

[35] O. Priya, R. Kumar Singh, S. Bhushan Das, V. Kumar, S. Farozan, Optimization of the structural, optical, and magnetic properties of sol-gel derived La^{3+} substituted nanostructured barium hexaferrites, Phys. Scr. 98 (2023), https://doi.org/10.1088/1402-4896/acd728.

[36] Z. Vakil, A. Kumar, A. Jain, K.M. Gupta, Effect of Cerium (Ce^{3+}) doping on structural, magnetic and dielectric properties of barium ferrite ($BaFe_{12}O_{19}$), in: IEEE International Conference on Electrical, Computer and Communication Technologies (ICECCT), 2015, pp. 1–4, https://doi.org/10.1109/ICECCT.2015.7225982.

[37] P. Marawichayo, W. Keawwattana, N. Koonsaeng, P. Jantaratana, Study the effect of the substitution of Ba with Pr in barium ferrite powder on magnetic properties, Adv. Mater. Res. 1025 (2014) 440–444, https://doi.org/10.4028/www.scientific.net/AMR.1025-1026.440.

[38] W. Chen, W. Wu, M. Mao, C. Zhou, S. Zhou, M. Li, Q. Wang, Improvement of the magnetization of barium hexaferrites induced by substitution of Nd^{3+} ions for Fe^{3+} ions, J. Supercond. Nov. Magn. 30 (2016) 707–714, https://doi.org/10.1007/s10948-016-3886-3.

[39] A. Zafar, A. Rahman, S. Shahzada, S. Anwar, M. Khan, A. Nisar, M. Ahmad, S. Karim, Electrical and magnetic properties of nano-sized Eu doped barium hexaferrites, J. Alloy. Compd. 727 (2017) 683–690, https://doi.org/10.1016/j.jallcom.2017.08.180.

[40] M.F. Ramírez-Ayala, A. Lobo Guerrero, A.M. Herrera-González, T.J. Pérez-Juache, R. López-Juárez, J.T. Elizalde-Galindo, V.E. Salazar-Muñoz, S. A. Palomares-Sánchez, S.Y. Reyes-López, Study of neodymium addition on the magnetic and structural properties of strontium hexaferrite synthesized by the Pechini method, J. Magn. Magn. Mater. 582 (2023) 170985, https://doi.org/10.1016/j.jmmm.2023.170985.

[41] M.M. Hessien, N. El-Bagoury, M.H.H. Mahmoud, M. Alsawat, A.K. Alanazi, M. M. Rashad, Implementation of La^{3+} ion substituted M-type strontium hexaferrite powders for enhancement of magnetic properties, J. Magn. Magn. Mater. 498 (2020) 166187, https://doi.org/10.1016/j.jmmm.2019.166187.

[42] C. Lei, S. Tang, Y. Du, Synthesis of aligned La^{3+}-substituted Sr-ferrites via molten salt assisted sintering and their magnetic properties, Cer. Int. 42 (2016) 15511–15516, https://doi.org/10.1016/j.ceramint.2016.06.204.

[43] E. Govea-Alcaide, J. Matilla-Arias, F. Guerrero, P. Mariño-Castellanos, K. Montero-Rey, F. Rosales-Saiz, I.F. Machado, Structural and magnetic properties of La-doped strontium-hexaferrites ceramics obtained by spark-plasma sintering, J. Magn. Magn. Mater. 533 (2021) 167966, https://doi.org/10.1016/j.jmmm.2021.167966.

[44] J. Lakshmikantha, G. Krishnamurthy, R. Hanumantha Nayak, N. Malathesh Pari, N.N. Ranjitha, Synthesis, structure, thermal, magnetic, dielectric properties of Ce^{3+} doped M-type $SrFe_{12}O_{19}$ and electrochemical determination of L-cysteine, Inorganic Chem. Commun. 146 (2022) 110175, https://doi.org/10.1016/j.inoche.2022.110175.

[45] Z. Zhou, Z. Wang, X. Wang, X. Wang, J. Zhang, F. Dou, M. Jin, J. Xu, Differences in the structure and magnetic properties of $Sr_{1-x}RE_xFe_{12}O_{19}$ (RE: Pr and Dy) ferrites by microwave-assisted synthesis method, J. Alloy. Compd. 610 (2014) 264–270, https://doi.org/10.1016/j.jallcom.2014.04.217.

[46] M. Hashim, S.J. Salih, M.M. Ismail, A. Ahmed, S. Singh Meena, A.A. Gaikwad, R. B. Jotania, S. Kumar, D. Ravinder, R. Kumar, A. Imran, K. Mujasam Batoo, S. E. Shirsath, Effect of lightly substituted samarium ions on the structural, optical, magnetic and dielectric properties of the sonochemically synthesized M-type Sr-hexaferrite nanoparticles, Physica B Condens. Matter. 681 (2024) 415840, https://doi.org/10.1016/j.physb.2024.415840.

[47] G.L. Tan, W. Li, Ferroelectricity and ferromagnetism of M-type lead hexaferrite, J. Am. Ceram. Soc. 98 (2015) 1812–1817, https://doi.org/10.1111/jace.13530.

[48] H.M. Umair, I. Bibi, F. Majid, A. Dahshan, S. Kamal, K. Jilani, S. Nouren, Z. Nazer, M. Iqbal, N. Alwadai, Synthesis of Dy-doped calcium hexaferrite ($CaDy_xF_{12-x}O_{19}$) nanoparticles and their ferroelectric, dielectric, magnetic and photocatalytic properties under solar light irradiation, J. Alloy. Compd. 999 (2024) 174893, https://doi.org/10.1016/j.jallcom.2024.174893.

[49] J. Mahapatro, S. Agrawal, Influence of erbium substitution on structural, optical and dielectric properties of strontium hexaferrite, Bull. Mater. Sci. 47 (2024) 26, https://doi.org/10.1007/s12034-023-03093-0.

[50] A. Hashhash, A. Hassen, W.S. Baleidy, H.S. Refai. Impact of rare-earth ions on the physical properties of hexaferrites $Ba_{0.5}Sr_{0.5}RE_{0.6}Fe_{11.4}O_{19}$, (RE = La, Yb, Sm, Gd, Er, Eu, and Dy). J. Alloys Compd. 873 (2021) 159812. https://doi.org/10.1016/j.jallcom.2021.159812.

[51] C.A. Stergiou, I. Manolakis, T.V. Yioultsis, G. Litsardakis, Dielectric and magnetic properties of new rare-earth substituted Ba-hexaferrites in the 2–18 GHz frequency range, J. Magn. Magn. Mater. 322 (2010) 1532–1535, https://doi.org/10.1016/j.jmmm.2009.07.082.

[52] K. Su, K. Yuan, Z. Guo, Y. He, Structure and magnetic studies of gadolinium doped M-type barium hexagonal ferrite, Trans. Metals Alloys 1 (2022) 1–8, https://doi.org/10.23977/trama.2022.010101.

[53] M. Kumar Manglam, M. Kar, Effect of Gd doping on magnetic and MCE properties of M-type barium hexaferrite, J. Alloy. Compd. 899 (2022) 163367, https://doi.org/10.1016/j.jallcom.2021.163367.

[54] S. Anjum, A. Seher, A.Z. Mustafa, Effect of La^{3+} ions substituted M-type barium hexa-ferrite on magnetic, optical, and dielectric properties, Appl. Phys. A 125 (2019) 664, https://doi.org/10.1007/s00339-019-2937-6.

[55] S. Kumar, M. Kumar Manglam, S. Supriya, H. Kumar Satyapal, R. Kumar Singh, M. Kar, Lattice strain mediated dielectric and magnetic properties in La doped barium hexaferrite, J. Magn. Magn. Mater. 473 (2019) 312–319, https://doi.org/10.1016/j.jmmm.2018.10.085.

[56] S. Anjum, M. Sattar, Z. Mustafa, Structural, optical and multiferroic properties of La^{+3}-substituted M-type barium hexaferrite propertiesBa$La_xFe_{12-x}O_{19}$, J. Mater. Sci. Mater. Electron. 32 (2021) 232–245, https://doi.org/10.1007/s10854-020-04759-9.

[57] I.G. Agung Putra Adnyana, K. Ngurah Suarbawa, W. Ari Adi, N. Nyoman Susi K. Wardani, L. Laudensia Senly Jalut. The effect of lanthanum substitution on coercivity field in oxide permanent magnet based on $Ba_{1-x}La_xFe_{12}O_{19}$ (x = 0; 0.02; 0.04; and 0.08). Int. J. Phys. Sci. Eng. 3 (2019) 42-49. https://doi.org/10.29332/ijpse.v3n1.281.

[58] S. Verma, O.P. Pandey, A.P. Jr, P. Sharma, Comparison of structural and magnetic properties of La^{3+} substituted $BaFe_{12}O_{19}$ prepared by different substitution methods, Physica b: Condensed Matter 448 (2014) 57–59, https://doi.org/10.1016/j.physb.2014.03.035.

[59] İ. Araz, Electromagnetic properties of Ce substituted barium hexaferrite in X band frequencies, J. Mater. Sci.: Mater. Elec. 30 (2019) 14935–14943, https://doi.org/10.1007/s10854-019-01866-0.

[60] Z. Mosleh, P. Kameli, A. Poorbaferani, M. Ranjbar, H. Salamati, Structural, magnetic and microwave absorption properties of Ce-doped barium hexaferrite, J. Magn. Magn. Mater. 397 (2016) 101–107, https://doi.org/10.1016/j.jmmm.2015.08.078.

[61] H.M.N. Samiullah, ul Huda Khan Asghar, Z. Abbas Gilani, M. Khalid, A. Ahmed, A. Kareem Khan, M. Rizwan Khan, F. Ahmed Sheikh, N. Ahmad, R. Busquets, Structural, dielectric, impedance and electric modulus properties of praseodymium-substituted $BaPr_xFe_{12-X}O_{19}$ nanoparticles synthesized via sol–gel method, Appl. Phys. A 128 (2022) 762, https://doi.org/10.1007/s00339-022-05799-0.

[62] S. Goel, A. Garg, R. Kumar Gupta, A. Dubey, N.E. Prasad, S. Tyagi, Effect of neodymium doping on microwave absorption property of barium hexaferrite in X-band, Mater. Res. Express 7 (2020) 016109, https://doi.org/10.1088/2053-1591/ab6544.

[63] P.S. Suprapedi, R. Muljadi, T. Sembiring, Synthesis and characterization of Ba-Ferrite with variation of Nd_2O_3 additive by powder metallurgy method, IOP Conf. Series: J. Phys.: Conf. Series 1204 (2019) 012016, https://doi.org/10.1088/1742-6596/1204/1/012016.

[64] H. Kumar Satyapal, R. Kumar Singh, S. Sonu Kumar, S. Bhushan Das, Tuning the structural, magnetic and multiferroic properties of Sm^{3+} substituted barium hexaferrites $BaFe_{12-x}Sm_xO_{19}$ nanoceramics, Mater. Today Proc. 44 (2021) 1833–1840, https://doi.org/10.1016/j.matpr.2020.12.011.

[65] S. Shan, J. Li, X. Zhao, S. Pi, S. Ma, Q. Wang, H. Liu, B. Wei, Y. Zhang, Magnetic properties of Sm-doped M-type barium ferrite by high-energy ball mill-assisted

solid-phase reaction method, J. Magn. Magn. Mater. 589 (2024) 171558, https://doi.org/10.1016/j.jmmm.2023.171558.
[66] F. Khademi, A. Poorbafrani, P. Kameli, H. Salamati, Structural, magnetic and microwave properties of Eu-doped barium hexaferrite powders, J. Supercond. Nov. Magn. 25 (2012) 525–531, https://doi.org/10.1007/s10948-011-1323-1.
[67] S. Mahadevan, A. Ravi Sankar, S. Singh, P. Sharma, Enhanced X-band absorption and shielding performance of Gd-substituted barium hexaferrite, J. Alloy. Compd. 959 (2023) 170456, https://doi.org/10.1016/j.jallcom.2023.170456.
[68] G. Murtaza Rai, M.A. Iqbal, K.T. Kubra, Effect of Ho^{3+} substitutions on the structural and magnetic properties of $BaFe_{12}O_{19}$ hexaferrites, J. Alloy. Compd. 495 (2010) 229–233, https://doi.org/10.1016/j.jallcom.2010.01.133.
[69] B.H. Bhat, B. Want, Magnetic behaviour of Neodymium-substituted strontium hexaferrite, Appl. Phys. A 122 (2016) 148, https://doi.org/10.1007/s00339-016-9687-5.
[70] J. Lakshmikantha, G. Krishnamurthy, B.M. Nagabhushan, E. Melagiriyappa, Dielectric properties and magnetic behavior of Gd^{3+} substituted M-type $SrFe_{12}O_{19}$ nanoferrites by auto combustion method using urea and citric acid mixtures as a dual fuel, J. Solid State Chem. 315 (2022) 123465, https://doi.org/10.1016/j.jssc.2022.123465.
[71] S.S. Kumar, R.K. Singh, A. Manash, G. Kumar, U. Shankar, H.K. Satyapal, Investigating structural, magnetic and multiferroic properties of gadolinium substituted strontium hexaferrite ($SrFe_{12-x}Gd_xO_{19}$), IOP Conf. Ser.: Mater. Sci. Eng. 1149 (2021) 012013, https://doi.org/10.1088/1757-899X/1149/1/012013.
[72] M.A. Almessiere, Y. Slimani, A. Baykal, Structural and magnetic properties of Ce-doped strontium hexaferrite, Cer. Inter. 44 (2018) 9000–9008, https://doi.org/10.1016/j.ceramint.2018.02.101.
[73] M.F. Ramírez-Ayala, A. Lobo Guerrero, J.L. Umapada Pal, M.L. Pérez-Mazariego, D.-A. Marquina, Effect of rare earth substitution on magnetic properties of strontium hexaferrite prepared by Pechini method, J. Alloy. Compd. 1002 (2024) 175388, https://doi.org/10.1016/j.jallcom.2024.175388.
[74] M.A. Almessiere, Y. Slimani, M. Sertkol, H. Gungunes, Y.S. Wudil, A. Demir Korkmaz, A. Baykal, Impact of Gd substitution on the structure, hyperfine interactions, and magnetic properties of Sr hexaferrites, Cer. Inter. 47 (2021) 33853–33864, https://doi.org/10.1016/j.ceramint.2021.08.297.
[75] G.P. Nethala, R. Tadi, G.R. Gajula, K.N. Chidambara Kumar, V. Veeraiah, Investigations on the structural, magnetic and mossbauer properties of cerium doped strontium ferrite, Physica b: Condensed Matter 550 (2018) 136–144, https://doi.org/10.1016/j.physb.2018.08.035.
[76] J. Hu, C. Liu, X. Kan, X. Liu, S. Feng, Q. Lv, Y. Yang, W. Wang, M. Shezad, K.M. Ur Rehman, Structure and magnetic performance of Gd substituted Sr-based hexaferrites, J. Alloy. Compd. 820 (2020) 153180, https://doi.org/10.1016/j.jallcom.2019.153180.
[77] K.M.U. Rehman, M. Riaz, X. Liu, M.W. Khan, Y. Yang, K.M. Batoo, S.F. Adil, M. Khan, Magnetic properties of Ce doped M-type strontium hexaferrites synthesized by ceramic route, J. Magn. Magn. Mater. 474 (2019) 83–89, https://doi.org/10.1016/j.jmmm.2018.10.087.
[78] V. Banihashemi, M.E. Ghazi, M. Izadifard, Structural, optical, dielectric and magnetic properties of Ce-doped strontium hexaferrite synthesized by a hydrothermal process, Mater. Sci.: Mater. Electron. 30 (2019) 17374–17381, https://doi.org/10.1007/s10854-019-02086-2.
[79] B. Want, B. Hamid Bhat, B. Zahoor Ahmad, Effect of lanthanum substitution on dielectric relaxation, impedance response, conducting and magnetic properties of strontium hexaferrite, J. Alloys Comp. 627 (2015) 78–84, https://doi.org/10.1016/j.jallcom.2014.11.065.
[80] A. Thakur, R.R. Singh, P.B. Barman, Structural and magnetic properties of La^{3+} substituted strontium hexaferrite nanoparticles prepared by citrate precursor method, J. Magn. Magn. Mater. 326 (2013) 35–40, https://doi.org/10.1016/j.jmmm.2012.08.038.
[81] W. Onreabroy, K. Papato, G. Rujijanagul, K. Pengpat, T. Tunkasiri, Study of strontium ferrites substituted by lanthanum on the structural and magnetic properties, Cer. Inter. 38 (2012) S415–S419, https://doi.org/10.1016/j.ceramint.2011.05.023.
[82] G.A. Al-Garalleh, I. Bsoul, Y. Maswadeh, E. Al-Hwaitat, S.H. Mahmood, Effects of synthesis route on the structural and magnetic properties of $Sr_{1-x}RE_xFe_{12}O_{19}$ nanocrystalline hexaferrites, Appl. Phys. A 125 (2019) 467, https://doi.org/10.1007/s00339-019-2762-y.
[83] Z. Rasouli, M. Yousefi, M. Bikhof Torbati, S. Samadi, K. Kalateh, Structural, magnetic, and microwave absorption properties of $SrCe_xFe_{12-x}O_{19}$/PVP composites. J. Microw, Power Electromagn Energy 54 (2020) 19–34, https://doi.org/10.1080/08327823.2020.1714104.
[84] X. Yang, Z. Chen, D. Zhou, X. Xiong, X. Jing, T. Zhao, H. Gong, B. Shen, Effect of the interaction of Fe- and Ce-contents on the structure and magnetic properties of M-type strontium ferrites, Cer. Inter. 50 (2024) 32465–32476, https://doi.org/10.1016/j.ceramint.2024.06.055.
[85] S. Pi, J. Li, Y. Zhang, W. Zhou, S. Shan, X. Zhao, Effects of Ce doping on the structure, morphology, and magnetic properties of M-type strontium ferrite, J. Supercond. Nov. Magn. (2024), https://doi.org/10.1007/s10948-024-06822-6.
[86] J. Lakshmikantha, G. Krishnamurthy, B.M. Nagabhushan, C.S. Naveen, E. Melagiriyappa, Effect of Ce^{3+} Substitution on Sr^{2+}; structural and magnetic properties of nanocrystalline $SrFe_{12}O_{19}$ hexaferrites prepared by self-propagation method using mixed fuels, J. Supercond. Nov. Magn. 35 (2022) 2485–2492, https://doi.org/10.1007/s10948-022-06223-7.
[87] X.D. Jing, Z.G. Li, Z.T. Chen, Z.Y. Li, C.Y. Qin, H.Y. Gong, Effect of praseodymium valence change on the structure, magnetic, and microwave absorbing properties of M-type strontium ferrite: the mechanism of influence of citric acid dosage and calcination temperature, Mater. Today Chem. 30 (2023) 101537, https://doi.org/10.1016/j.mtchem.2023.101537.
[88] E. Demir, S. Emre Sünbül, K. İçin, Exploring the effects of annealing temperature on structural and magnetic properties of low-level neodymium-substituted strontium hexaferrite synthesized Via combustion method, J. Mat. Mechatronics: A 4 (2023) 446–458, https://doi.org/10.55546/jmm.1319818.
[89] M. Effendi, E. Solihah, C. Kurniawan, W. Tri Cahyanto, W. Widanarto, Transformation of structure, magnetic properties and microwave absorption capability in Nd-doped strontium hexaferrite, Key Eng. Mater. 855 (2020) 255–260, https://doi.org/10.4028/www.scientific.net/KEM.855.255.
[90] A.M. Semaida, M.A. Darwish, M.M. Salem, D. Zhou, T.I. Zubar, S.V. Trukhanov, A.V. Trukhanov, V.P. Menushenkov, A.G. Savchenko, Impact of Nd^{3+} substitutions on the structure and magnetic properties of nanostructured $SrFe_{12}O_{19}$ hexaferrite, Nanomater. 12 (2022) 3452, https://doi.org/10.3390/nano12193452.
[91] N. Yasmin, M. Mirza, M. Safdar, M. Zahid, M. Ahmad, M.S. Awan, M. Altaf, Influence of samarium substitution on the structural and magnetic properties of M-type hexagonal ferrites, J. Magn. Magn. Mater. 446 (2018) 276–281, https://doi.org/10.1016/j.jmmm.2017.09.005.
[92] M. Sattar, S. Anjum, M. Yasin Raja, Z. Mustafa, A. Mansoor, R. Khurram, T. Ilayas, Samarium substituted M-type Sr hexaferrites: The structural, magnetic and electrochemical properties for supercapacitor applications, Cer. Inter. 50 (2024) 16747–16764, https://doi.org/10.1016/j.ceramint.2024.01.224.
[93] C. Liu, X. Kan, X. Liu, S. Feng, J. Hu, W. Wang, K. Mehmood Ur Rehman, M. Shezad, Influence of the Eu substitution on the structure and magnetic properties of the Sr-hexaferrites, Cer. Inter. 46 (2020) 171–179, https://doi.org/10.1016/j.ceramint.2019.08.245.
[94] A.M. Adam, A. Elshafaie, E.M.M. Ibrahim, Structural and magnetic properties of Dy doped $SrFe_{12}O_{19}$ ferrites, Mater. Today Commun. 35 (2023) 105884, https://doi.org/10.1016/j.mtcomm.2023.105884.
[95] Z. Chen, Bo Xu, Z. Li, N. Zhou, H. Gong, X. Jing, The influence of Ho doping on the morphology and magnetic properties of M-type strontium ferrite with different Fe/Sr, Mater. Chem. Phys. 312 (2024) 128635, https://doi.org/10.1016/j.matchemphys.2023.128635.
[96] M. Mahdiani, A. Sobhani, F. Ansari, M. Salavati-Niasari, Lead hexaferrite nanostructures: green amino acid sol–gel autocombustion synthesis, characterization and considering magnetic property, J. Mater. Sci. Mater. Electron. 28 (2017) 17627–17634, https://doi.org/10.1007/s10854-017-7701-0.
[97] S. Prathap, W. Madhuri, S. Singh Meena, Effect of non-stoichiometry in lead hexaferrites on magnetic and dielectric properties, Mater. Chem. Phys. 220 (2018) 137–148, https://doi.org/10.1016/j.matchemphys.2018.08.034.
[98] A.L. Guerrero, M. Mirabal-García, S.A. Palomares-Sánchez, J.R. Martínez, Effect of Pb on the magnetic interactions of the M-type hexaferrites, J. Magn. Magn. Mater. 399 (2016) 41–45, https://doi.org/10.1016/j.jmmm.2015.09.052.
[99] F. Ansari, F. Soofivand, M. Salavati-Niasari, Utilizing maleic acid as a novel fuel for synthesis of $PbFe_{12}O_{19}$ nanoceramics via sol–gel auto-combustion route, Mater. Char. 103 (2015) 11–17, https://doi.org/10.1016/j.matchar.2015.03.010.
[100] S.E. Mousavi Ghahfarokh, Z.A. Rostami, I. Kazeminezhad, Fabrication of $PbFe_{12}O_{19}$ nanoparticles and study of their structural, magnetic and dielectric properties, J. Magn. Magn. Mater. 399 (2016) 130–142, https://doi.org/10.1016/j.jmmm.2015.09.063.
[101] S. Kumar Godara, R. Himanshi, V. Jasrotia, P.S. Kaur, J. Malhi, A. Ahmed, S. Kandwal, M. Verma, Singh, P.T. Kaur, R. Kumar Dhaka, K. Chuchra, A.H. S. Rana, A. Kumar Sood, K. Sharma, S. Dhaka, A. Verma, A sustainable approach for the synthesis of $PbFe_{12}O_{19}$ materials using tomato pulp as a fuel: Structural, morphological, optical, magnetic, and dielectric traits, J. Magn. Magn. Mater. 573 (2023) 170643, https://doi.org/10.1016/j.jmmm.2023.170643.
[102] A.L. Guerrero-Serrano, M. Mirabal-García, S.A. Palomares-Sánchez, Synthesis and study of the lanthanum substitution in the lead M-Type hexaferrite, J. Supercond. Nov. Magn. 27 (2014) 1709–1713, https://doi.org/10.1007/s10948-014-2489-0.
[103] K. Husain, S. Ullah Asif, E. Abdu Musad Saleh, R.H. Althomali, M.M. Moharam, Ismail Hasan, Samarium substituted M-type Ca-hexaferrites: Structural and magnetic features, Inorg. Chem. Commun. 165 (2024) 112493, https://doi.org/10.1016/j.inoche.2024.112493.
[104] L. Khanna, N.K. Verma, Size-dependent magnetic properties of calcium ferrite nanoparticles, J. Magn. Magn. Mater. 336 (2013) 1–7, https://doi.org/10.1016/j.jmmm.2013.02.016.
[105] S. Kumar, S. Ahmad Bhat, S. Chaurasiya, G. Ahamed Lone, A. Rashid, P. Kumar Sharma, M. Ikram, Investigation on the structural, morphological and magnetic properties of $Ca_{1-x}Eu_xFe_{12-y}Ti_yO_{19}$ hexaferrite system, Solid State Sci. 145 (2023) 107337, https://doi.org/10.1016/j.solidstatesciences.2023.107337.
[106] M. Al-Dossari, T. Anwar, A.M. Saeedi, R.H. Althomali, G.F.B. Solre, S. Ullah Asif, I. Ahmed, F. Nosheen, Structural and magnetic aspects of aluminium substituted dual lanthanum and calcium based hexaferrite nanoparticles for magnetic applications, Mater. Sci. Eng. B 310 (2024) 117709, https://doi.org/10.1016/j.mseb.2024.117709.
[107] V.S. Shinde, S.G. Dahotre, L.N. Singh, Synthesis and characterization of La substituted M type calcium hexaferrite. i-manager's, J. Mater. Sci. 7 (2019) 10–17. https://imanagerpublications.com/assets/pdfDownload/JMS/2019/7_2JMS_September_2019/JMSSeptember19RP02.pdf.
[108] N. Ramu, K. Meera, R. Ranjith, R. Muralidharan, The role of B-site substitution on the structural and dielectric properties of samarium orthoferrite polycrystals, Mater. Res. Express 6 (2019) 036106, https://doi.org/10.1088/2053-1591/aaf6d0.
[109] L. Guganathan, C. Rajeevgandhi, K. Sathiyamurthy, K. Thirupathi, M. Santhamoorthy, E. Chinnasamy, C. Jayprakash Raorane, V. Raj, S. Cheol Kim,

P. Anand, Magnetic application of gadolinium orthoferrite nanoparticles synthesized by sol–gel auto-combustion method, Gels 8 (2022) 688, https://doi.org/10.3390/gels8110688.
[110] D. Seifert, J. Töpfer, M. Stadelbauer, R. Grössinger, J.M. Le Breton, Rare-earth-substituted $Sr_{1-x}Ln_xFe_{12}O_{19}$ hexagonal ferrites, J. Am. Cer. Soc. 94 (2022) 2109–2118, https://doi.org/10.1111/j.1551-2916.2010.04363.x.
[111] H. Zhang, D. Zeng, Z. Liu, The law of approach to saturation in ferromagnets originating from the magnetocrystalline anisotropy, J. Magn. Magn. Mater. 322 (2010) 2375–2380, https://doi.org/10.1016/j.jmmm.2010.02.040.
[112] D. Seifert, J. Töpfer, F. Langenhorst, J.-M. Le Breton, H. Chiron, L. Lechevallier, Synthesis and magnetic properties of La-substituted M-type Sr hexaferrites, J. Magn. Magn. Mater. 321 (2009) 4045–4051, https://doi.org/10.1016/j.jmmm.2009.07.088.
[113] I. Sadiq, S. Naseem, M. Naeem Ashiq, M. Asif Iqbal, I. Ali, M.A. Khan, M. U. Shanawar Niaz, Rana, Spin canting effect and microwave absorption properties of Sm–Mn substituted nanosized material, J. Magn. Magn. Mater. 395 (2015) 159–165, https://doi.org/10.1016/j.jmmm.2015.04.118.
[114] X. Liu, W. Zhong, S. Yang, Z. Yu, B. Gu, Y. Du, Influences of La^{3+} substitution on the structure and magnetic properties of M-type strontium ferrites, J. Magn. Magn. Mater. 238 (2002) 207–214, https://doi.org/10.1016/S0304-8853(01)00914-3.
[115] U. Topal, Factors influencing the remanent properties of hard magnetic barium ferrites: Impurity phases and grain sizes, J. Magn. Magn. Mater. 320 (2008) 331–335, https://doi.org/10.1016/j.jmmm.2007.06.025.
[116] F. Wang, K. Chen, J. Du, J. Zhang, Simultaneous increase in remanence and coercivity during grain refining of Nd-Fe-B deformed magnets, J. Rare Earths 40 (2022) 1763–1771, https://doi.org/10.1016/j.jre.2021.10.008.
[117] N. Adeela, U. Khan, M. Iqbal, S. Riaz, M. Irfan, H. Ali, K. Javed, I. Bukhtiar, K. Maaz, S. Naseem, Structural and magnetic response of Mn substituted Co_2 Y-type barium hexaferrites, J. Alloy. Compd. 686 (2016) 1017–1924, https://doi.org/10.1016/j.jallcom.2016.06.239.
[118] U. Kurtan, R. Topkaya, A. Baykal, M.S. Toprak, Temperature dependent magnetic properties of $CoFe_2O_4$/CTAB nanocomposite synthesized by sol–gel auto-combustion technique, Cer. Int. 39 (2013) 6551–6558, https://doi.org/10.1016/j.ceramint.2013.01.088.
[119] R. Murillo-Ortíz, M. Mirabal-García, J.M. Martínez-Huerta, J.G. Cabal Velarde, I. E. Castaneda-Robles, A. Lobo-Guerrero, Analysis of the magnetic properties in hard-magnetic nanofibers composite, J. Appl. Phys. 123 (2018) 105108, https://doi.org/10.1063/1.5008368.
[120] M.A. Almessiere, Y. Slimani, S. Güner, J. van Leusen, A. Baykal, P. Kögerler, Effect of Nb^{3+} ion substitution on the magnetic properties of $SrFe_{12}O_{19}$ hexaferrites, J. Mater. Sci. Mater. Electron. 30 (2019) 11181–11192, https://doi.org/10.1007/s10854-019-01464-0.
[121] M.A. Almessiere, A.D. Korkmaz, Y. Slimani, M. Nawaz, S. Ali, A. Baykal, Magneto-optical properties of rare earth metals substituted Co-Zn spinel nanoferrites, Ceram. Int. 45 (2019) 3449–3458, https://doi.org/10.1016/j.ceramint.2018.10.260.
[122] I. Ali, M.U. Islam, M.S. Awan, M. Ahmad, M. Naeem Ashiq, S. Naseem, Effect of Tb^{3+} substitution on the structural and magnetic properties of M-type hexaferrites synthesized by sol–gel auto-combustion technique, J. Alloy. Compd. 550 (2013) 564–572, https://doi.org/10.1016/j.jallcom.2012.10.121.
[123] A. Nag, R.S.C. Bose, K.S. Venu, H. Singh, Influence of particle size on magnetic and electromagnetic properties of hexaferrite synthesised by sol-gel auto combustion route, Cer. Inter. 48 (2022) 15303–15313, https://doi.org/10.1016/j.ceramint.2022.02.064.
[124] F. Holm Gjørup, M. Saura-Múzquiz, J. Voldum Ahlburg, H. Lyder Andersen, M. Christensen, Coercivity enhancement of strontium hexaferrite nano-crystallites through morphology controlled annealing, Materialia 4 (2018) 203–210, https://doi.org/10.1016/j.mtla.2018.09.017.
[125] D.L. Leslie-Pelecky, R.D. Rieke, Magnetic properties of nanostructured materials, Chem. Mater. 8 (1996) 1770–1783, https://doi.org/10.1021/cm960077f.
[126] L. Kumar, M. Kar, Effect of La^{3+} substitution on the structural and magnetocrystalline anisotropy of nanocrystalline cobalt ferrite ($CoFe_{2-x}La_xO_4$), Cer. Inter. 38 (2012) 4771–47782, https://doi.org/10.1016/j.ceramint.2012.02.065.
[127] K. Rana, S. Thakur, M. Tomar, V. Gupta, A. Thakur. Effect of low sintering temperature on the structural and magnetic properties of M-type strontium hexaferrite. J. Magn. Magn. Mater. 587 (23) 171289. https://doi.org/10.1016/j.jmmm.2023.171289.
[128] P. Kush Rana, M. Thakur, V. Tomar, A.T. Gupta, Investigation of cobalt substituted M-type barium ferrite synthesized via coprecipitation method for radar absorbing material in Ku-band (12–18 GHz), Cer. Inter. 44 (2018) 6370–6375, https://doi.org/10.1016/j.ceramint.2018.01.028.
[129] Kush Rana, Preeti Thakur, Atul Thakur, Monika Tomar, Vinay Gupta, Jean Luc Mattei, Patrick Queffelec. Influence of samarium doping on magnetic and structural properties of M type Ba–Co hexaferrite. Cer. Inter. 42 (2016) 8413-8418. https://doi.org/10.1016/j.ceramint.2016.02.058.